nature biomedical engineering

ARTICLES

https://doi.org/10.1038/s41551-021-00831-9

Check for updates

Intratumourally injected alum-tethered cytokines elicit potent and safer local and systemic anticancer immunity

Yash Agarwal[1,2], Lauren E. Milling[1,2], Jason Y. H. Chang[2,3], Luciano Santollani[2,4], Allison Sheen[1,2], Emi A. Lutz[1,2], Anthony Tabet[2,4], Jordan Stinson[1,2], Kaiyuan Ni[2], Kristen A. Rodrigues[2,3,5,6], Tyson J. Moyer[2,3], Mariane B. Melo[2,3], Darrell J. Irvine[1,2,3,6,7,8] ✉ and K. Dane Wittrup[1,2,4] ✉

Anti-tumour inflammatory cytokines are highly toxic when administered systemically. Here, in multiple syngeneic mouse models, we show that the intratumoural injection of recombinantly expressed cytokines bound tightly to the common vaccine adjuvant aluminium hydroxide (alum) (via ligand exchange between hydroxyls on the surface of alum and phosphoserine residues tagged to the cytokine by an alum-binding peptide) leads to weeks-long retention of the cytokines in the tumours, with minimal side effects. Specifically, a single dose of alum-tethered interleukin-12 induced substantial interferon-γ-mediated T-cell and natural-killer-cell activities in murine melanoma tumours, increased tumour antigen accumulation in draining lymph nodes and elicited robust tumour-specific T-cell priming. Moreover, intratumoural injection of alum-anchored cytokines enhanced responses to checkpoint blockade, promoting cures in distinct poorly immunogenic syngeneic tumour models and eliciting control over metastases and distant untreated lesions. Intratumoural treatment with alum-anchored cytokines represents a safer and tumour-agnostic strategy to improving local and systemic anticancer immunity.

Immune checkpoint blockade therapy has improved progression-free survival in patients suffering from cancer over previous treatment modalities[1–4]. However, immune checkpoint blockade typically elicits durable responses in a minority of patients, in part because of the highly immunosuppressive tumour microenvironment (TME)[5,6]. Although rational combinations with inflammatory cytokines or immune agonists can relieve some immunosuppression[7,8], systemic dosing of these proteins is impeded by severe immune-related adverse events. Early phase 1 clinical trials involving promising cytokines such as interleukin-2 (IL-2) and interleukin-12 (IL-12) resulted in sub-optimal anti-tumour efficacy with high treatment-related morbidity and even mortality, partially due to limited drug exposure within the tumour and over-stimulation of lymphocytes in healthy tissue[9–14]. Thus, there is great promise for strategies that could localize cytokine effects to the TME.

One approach to focus the activity of immunostimulatory agents in tumours while lowering systemic toxicity is to administer these drugs intratumourally. With advances in interventional radiology, endoscopy and laproscopic surgery procedures, most lesions in the human body are now accessible for intratumoural (i.t.) dosing[15]. Moreover, a locally stimulated immune response in one lesion can elicit systemic anti-tumour immunity to promote control over untreated lesions in patients, especially in combination with systemic checkpoint blockade therapy[16–19]. However, i.t. injection of therapeutics does not ensure persistence in the TME, since free drugs are quickly cleared via lymphatics and/or the tumour vasculature, rapidly leading to toxic accumulation in the circulation[20,21]. For instance, while there is extensive interest in the local delivery of IL-12[22–24], these approaches are typically accompanied by rapid leakage of IL-12 into the circulation, which in turn triggers systemic interferon-γ (IFN-γ) production (a biomarker for IL-12-related immune-related adverse events)[25–27]. We have previously reported a strategy of fusing cytokines to collagen-binding proteins to enhance TME retention following i.t. administration, which reduced toxicities of these potent agents while enhancing therapeutic efficacy[28]. This strategy extends drug persistence over a period of a few days, but is dose-limited by the quantity of collagen available in the TME, which varies from patient to patient and tumour to tumour. Further, drug is spatiotemporally governed by the distribution and turnover of collagen in the tumour.

In this Article, we demonstrate an approach for the i.t. delivery of engineered cytokines using the US Food and Drug Administration (FDA)-approved vaccine adjuvant aluminium hydroxide (alum). Alum has nearly 100 years of history of safe use in humans and is administered annually to millions of people in over 20 vaccine formulations. Aluminium hydroxide adjuvants are composed of micrometre-scale aggregates of nanometre-scale rod-shaped nanocrystals; these alum aggregates form a physical depot at injection sites in tissue that is persistent over a period of weeks[29]. Phosphorylated proteins bind tightly to alum through a ligand exchange reaction with surface hydroxyls, enabling retention of bound molecules in the presence of interstitial fluid in vivo[30–32]. To exploit this chemistry, we

[1]Department of Biological Engineering, Massachusetts Institute of Technology, Cambridge, MA, USA. [2]Koch Institute for Integrative Cancer Research, Massachusetts Institute of Technology, Cambridge, MA, USA. [3]Ragon Institute of Massachusetts General Hospital, Massachusetts Institute of Technology and Harvard University, Cambridge, MA, USA. [4]Department of Chemical Engineering, Massachusetts Institute of Technology, Cambridge, MA, USA. [5]Harvard-MIT Health Sciences and Technology Program, Institute of Medical Engineering and Science, Massachusetts Institute of Technology, Cambridge, MA, USA. [6]Consortium for HIV/AIDS Vaccine Development, The Scripps Research Institute, La Jolla, CA, USA. [7]Department of Materials Science and Engineering, Massachusetts Institute of Technology, Cambridge, MA, USA. [8]Howard Hughes Medical Institute, Chevy Chase, MD, USA. ✉e-mail: djirvine@mit.edu; wittrup@mit.edu

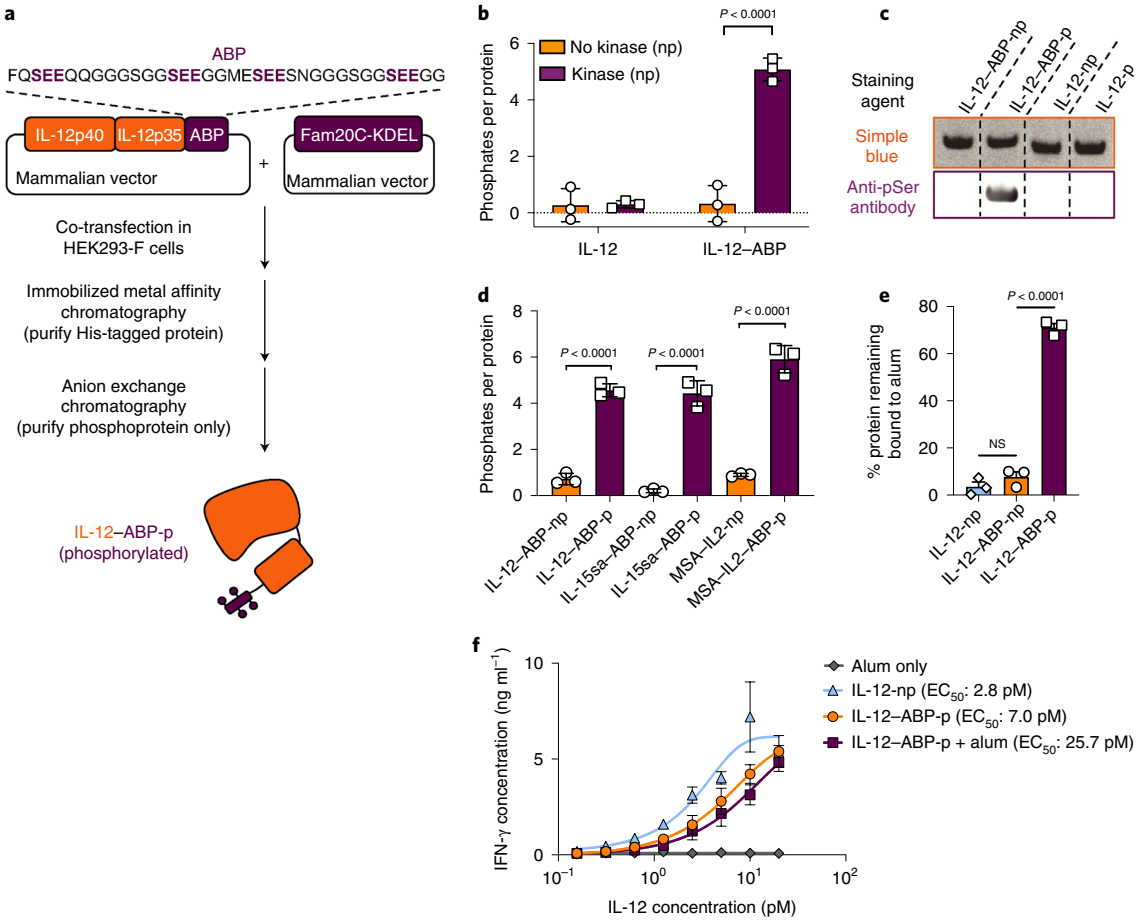

Fig. 1 | Co-expression of cytokines and Fam20C enables in-cell site-specific serine phosphorylation of interleukins. a, Manufacturing workflow for ABP-fusion proteins with IL-12 fused to ABP10 as an example. **b**, Phosphorylation as measured by malachite green assay for IL-12 and IL-12–ABP either expressed alone (np) or co-expressed with Fam20C-KDEL (p). **c**, Indicated proteins were run on an SDS–PAGE gel stained with Coomassie Blue (Simple Blue, orange) or transferred to a membrane and stained with an anti-pSer antibody followed by an IR800 secondary (purple). Shown are bands for ~65 kDa purified protein. The blot was analysed by Fiji (ImageJ). The unedited blot image is available as source data. **d**, Phosphorylation was measured as in **b** for indicated proteins. **e**, Fluorophore-conjugated IL-12 fusion proteins (10 μg ml^{-1}) were mixed with Alhydrogel (100 μg ml^{-1}) for 30 min in TBS, then incubated in 10% mouse serum in PBS for 1 h, followed by fluorescence spectroscopy to measure protein remaining bound to alum. **f**, IL-12 proteins at indicated concentrations (maximum alum concentration was 6 ng ml^{-1}) were incubated with murine splenocytes for two days. Shown are the IFN-γ concentrations measured in culture supernatants by ELISA. ABP refers specifically to ABP10. Data are representative of at least two independent experiments with $n = 3$ technical replicates per group and presented as mean ± s.d. *P* values were determined by ordinary one-way ANOVA followed by Tukey's multiple comparison test (**d**,**e**) or two-way ANOVA with Šídák's multiple comparisons test (**b**) using GraphPad PRISM, and exact *P* values are indicated (NS, not significant, $P > 0.05$).

developed an approach for in-cell site-specific protein phosphorylation to synthesize bioactive proteins fused with a phosphorylated alum-binding peptide (ABP) tag. We used this approach to produce a series of ABP-labelled cytokines, which rapidly adsorbed to alum after simple mixing, and upon i.t. injection were retained in tumours for more than a week. Applied to the cytokine IL-12, this approach dramatically increased i.t. retention of the cytokine and eliminated systemic toxicities seen upon i.t. injection of the free drug, while also increasing anti-tumour efficacy. Moreover, a single i.t. dose of alum-anchored IL-12 elicited strong IFN-γ-dependent collaboration between innate and adaptive immune cells, producing robust systemic anti-tumour responses in multiple poorly immunogenic preclinical models when combined with systemic checkpoint blockade therapy.

Results

Targeted phosphorylation via an in-cell approach is robust. A single kinase, Fam20C, is responsible for phosphorylation of the majority of the mammalian secreted phosphoproteome[33]. We hypothesized that co-expression of Fam20C together with therapeutic proteins fused to a short peptide containing consensus motifs for the kinase (alum binding peptide or ABP) would lead to the specific phosphorylation of the ABP (Fig. 1a). Fam20C recognizes and phosphorylates serines contained within a well-defined consensus motif (S-x-E) in mammalian cells[33,34], and can be engineered for retention in the endoplasmic reticulum using a KDEL C-terminal tag while still maintaining activity[33]. Thus, we designed an initial set of ABP peptides bearing S-x-E motifs based on naturally phosphorylated sequences[33] and co-expressed a single-chain form of mouse IL-12 fused to these ABPs together with Fam20C-KDEL in HEK293-F cells (Fig. 1a). The resulting IL-12–ABP proteins were purified by sequential immobilized metal affinity chromatography and anion exchange chromatography (Supplementary Fig. 1a–h). Anion exchange chromatography revealed a major product peak (P3, Supplementary Fig. 1f–h) that was the monomeric, fully phosphorylated IL-12–ABP. IL-12–ABP was phosphorylated when

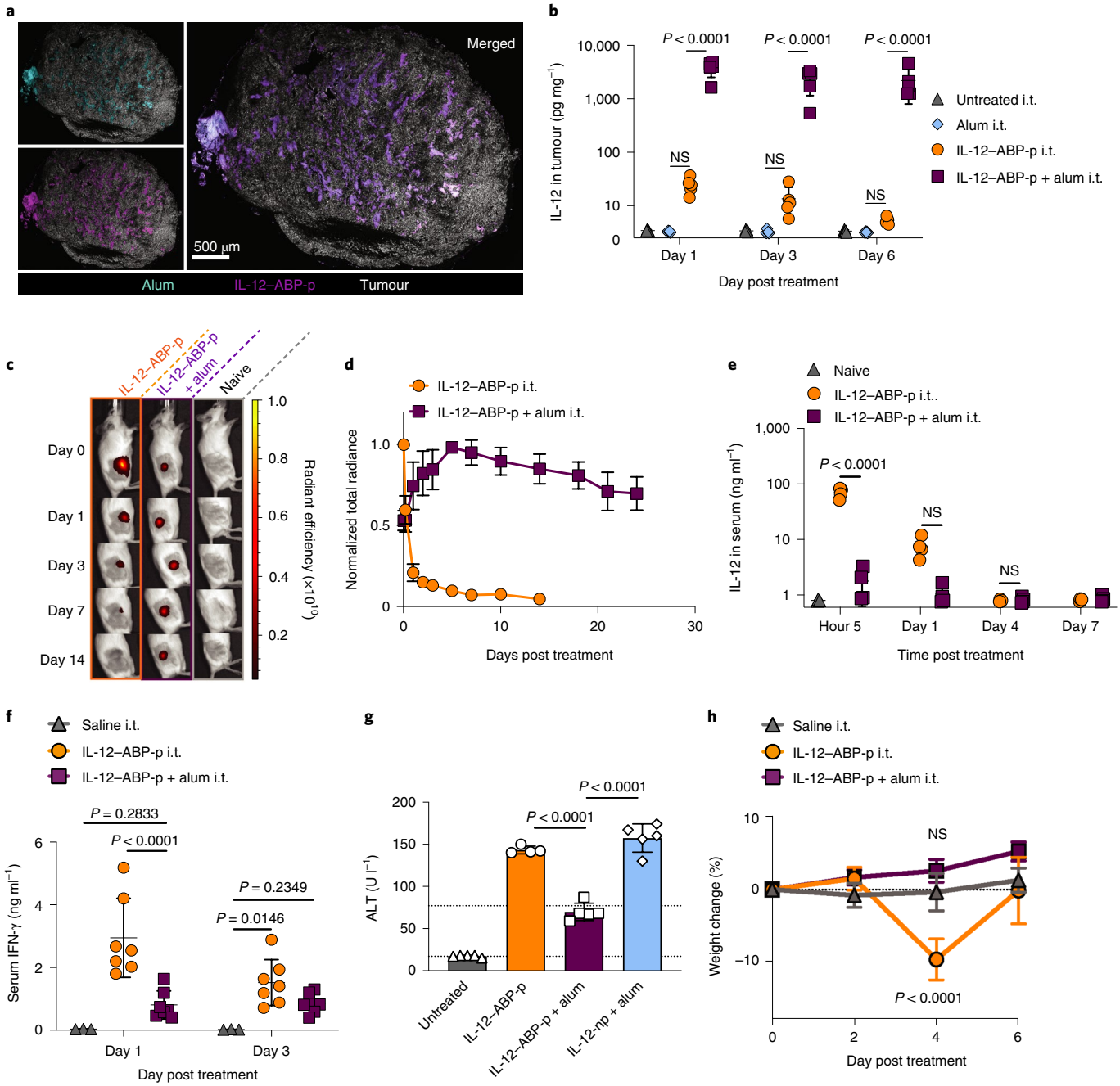

Fig. 2 | Alum-tethered IL-12 is retained locally and elicits negligible systemic toxicity after i.t. administration. a,**b**, C57Bl/6 mice bearing subcutaneous B16F10 tumours were treated with 20 μg AF568-labelled IL-12–ABP-p + 100 μg AF488-pSer$_4$-labelled alum intratumourally (**a**) or 20 μg IL-12–ABP-p + 100 μg alum intratumourally and 200 μg anti-PD1 i.p. (**b**). Shown are representative tumour histological sections 30 min after injection with IL-2 in magenta, alum in cyan and B16F10 tumour cells in white (scale bars, 0.5 mm) (**a**) and IL-12 levels ($n = 5$ animals per group) measured in tumour lysates at the indicated times (**b**). **c**–**e**, Albino B6 mice ($n = 4$–5 animals per group) bearing subcutaneous B16F10–Trp2 KO (unpigmented) tumours were treated intratumourally with 20 μg AF647-labelled IL-12–ABP-p alone (orange) or combined with 100 μg alum (purple). Shown are the representative IVIS images (**c**), quantification of i.t. AF647 fluorescence (**d**) and serum IL-12 levels (**e**) over time. **f**–**h**, C3H-Hej mice ($n = 5$–7 animals per group) with established Ag104A tumours were treated intratumourally with 20 μg IL-12 alone, 20 μg IL-12–ABP-p alone or IL-12–ABP-p mixed with 100 μg alum. Shown are serum IFN-γ levels (**f**), serum ALT concentration on day 3 post-treatment (**g**) and % change in body weight over time after treatment (**h**). All data are presented as mean ± s.d. with indicated *n*. ABP refers specifically to ABP10. *P* values were determined by ordinary one-way ANOVA (**g**) or two-way ANOVA (**b**,**f**,**h**) followed by Tukey's multiple comparison test, and two-way ANOVA followed by Holm–Šídák multiple comparison test (**e**) using GraphPad PRISM, and exact *P* values are indicated. *P* values for **h** were computed versus the saline i.t. group.

co-expressed with the kinase (IL-12–ABP-p) but not when expressed without kinase (IL-12–ABP-np), and IL-12 lacking the ABP was not phosphorylated regardless of the presence of the kinase (Fig. 1b,c). Phosphorylation was dependent on the presence of the target serines in the S-x-E motifs and was sensitive to the spacing between these motifs as well as the sequence of flanking residues (Supplementary

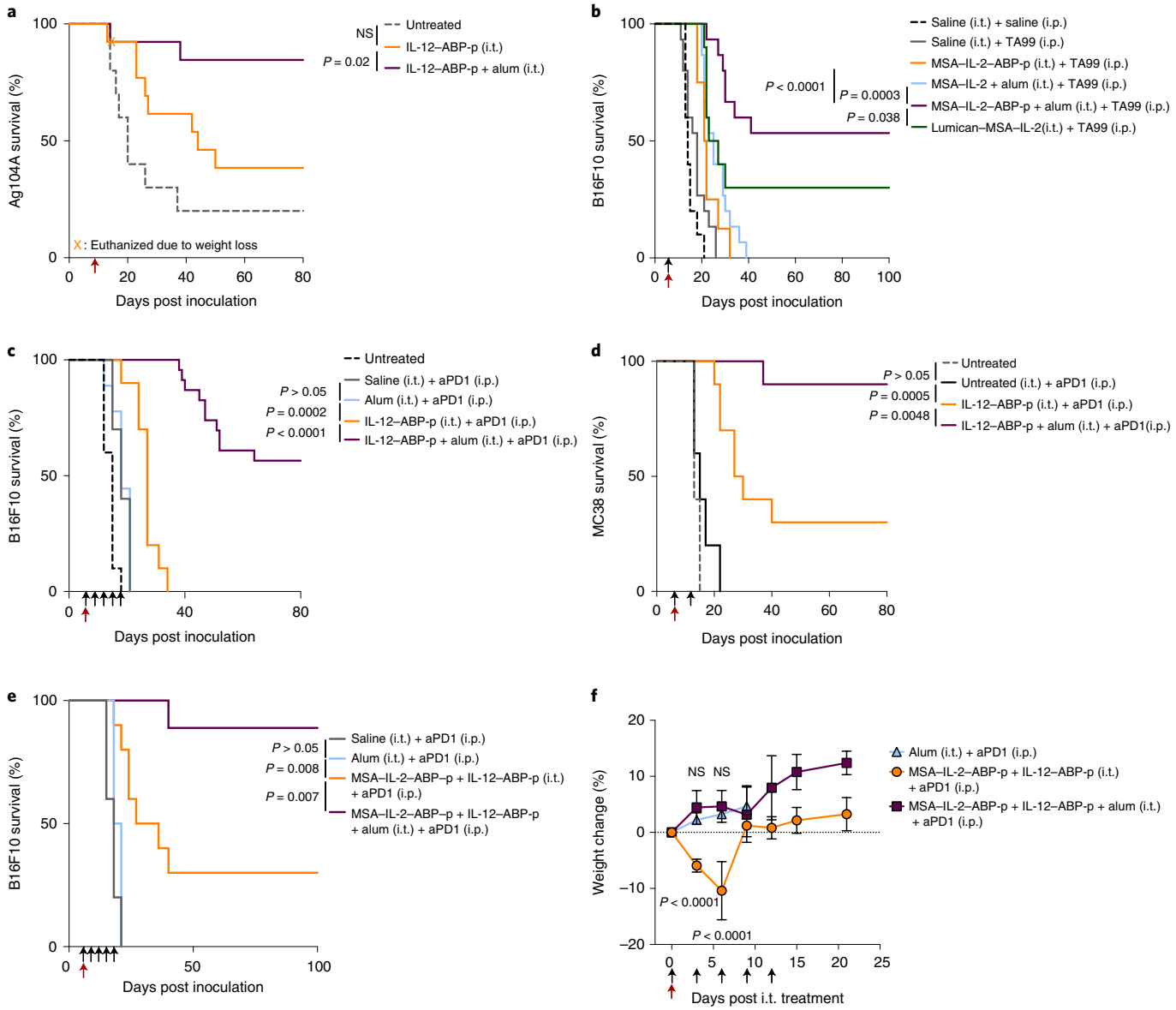

Fig. 3 | A single dose of alum-anchored i.t. IL-12 or IL-2 elicits long-term tumour regression in multiple syngeneic cancer models. a–d, Overall survival over time for mice bearing flank Ag104A (**a**), B16F10 (**b**,**c**) or MC38 (**d**) tumours after a single i.t. dose administered on day 7 (**a**,**d**) or day 6 (**b**,**c**) after inoculation. Groups for **a** were untreated ($n = 10$), IL-12-ABP-p (20 μg) i.t. ($n = 13$), and IL-12-ABP-p (20 μg)/alum (100 μg) i.t. ($n = 13$). Treatments for **b** were saline i.t. + saline i.p, ($n = 10$), saline i.t. + TA99 i.p. ($n = 15$), MSA-IL-2-ABP-p (36 μg) i.t. + TA99 i.p. ($n = 8$), MSA-IL-2 (34 μg)/alum (90 μg) i.t. + TA99 i.p. ($n = 15$), MSA-IL-2-ABP-p (36 μg)/alum (90 μg) i.t. + TA99 i.p. ($n = 15$), and lumican-MSA-IL-2 (52 μg) i.t. + TA99 i.p. ($n = 10$). TA99 was dosed at 200 μg per injection. Treatments for **c** were untreated ($n = 10$), saline i.t. + anti-PD1 i.p. ($n = 10$), alum (100 μg) i.t. + anti-PD1 i.p. ($n = 9$), IL-12-ABP-p (20 μg) i.t. ($n = 15$), and IL-12-ABP-p (20 μg)/alum (100 μg) i.t ($n = 28$). Treatments for **d** were untreated ($n = 5$), untreated i.t. + anti-PD1 i.p. ($n = 5$), IL-12-ABP-p (20 μg) i.t. ($n = 10$), and IL-12-ABP-p (20 μg)/alum (100 μg) i.t ($n = 20$). Anti-PD1 was dosed at 200 μg per injection. **e**,**f**, Mice with B16F10 tumours were treated on day 6 i.t. with saline ($n = 5$), alum (100 μg, $n = 5$), IL-12-ABP-p (20 μg) + MSA-IL-2-ABP-p (36 μg, $n = 10$), or IL-12-ABP-p + MSA-IL-2-ABP-p + alum ($n = 10$); all groups received anti-PD1 i.p. (black arrows). Shown is the overall survival (**e**) and percent change in body weight (mean ± s.d., **f**) over time after treatment. Anti-PD1 was administered on days 6, 9, 12, 15 and 18 for **b**,**f**,**g** and days 7 and 13 for **c**. Red and black arrows indicate timing of i.t. and i.p. treatments, respectively. ABP refers specifically to ABP10. *P* values were determined by the log-rank (Mantel–Cox) test (**a**,**c**,**d**), Gehan–Breslow-Wilcoxon test (**b**,**e**) or two-way ANOVA followed by Tukey's multiple comparison test versus alum i.t. at indicated timepoints (**f**) using GraphPad PRISM.

Fig. 1i–l). When fused to other therapeutic cytokines (IL-2 fused to mouse serum albumin (MSA, to enhance expression) or a super-agonist complex of interleukin-15 (IL-15) with the IL-15α chain (IL-15sa)), we observed consistent phosphorylation of the ABP (Fig. 1d), indicating that this in-cell Fam20C-dependent phosphorylation approach is robust and modular.

Initial adsorption of IL-12 to alum in buffer was similar irrespective of the presence of the ABP tag (Supplementary Fig. 2a). However, the majority of IL-12 with a phosphorylated ABP remained bound following incubation of the cytokine-loaded alum with mouse serum, while unphosphorylated IL-12 rapidly desorbed (Fig. 1e). Tracked over time, phosphorylated IL-12 was slowly

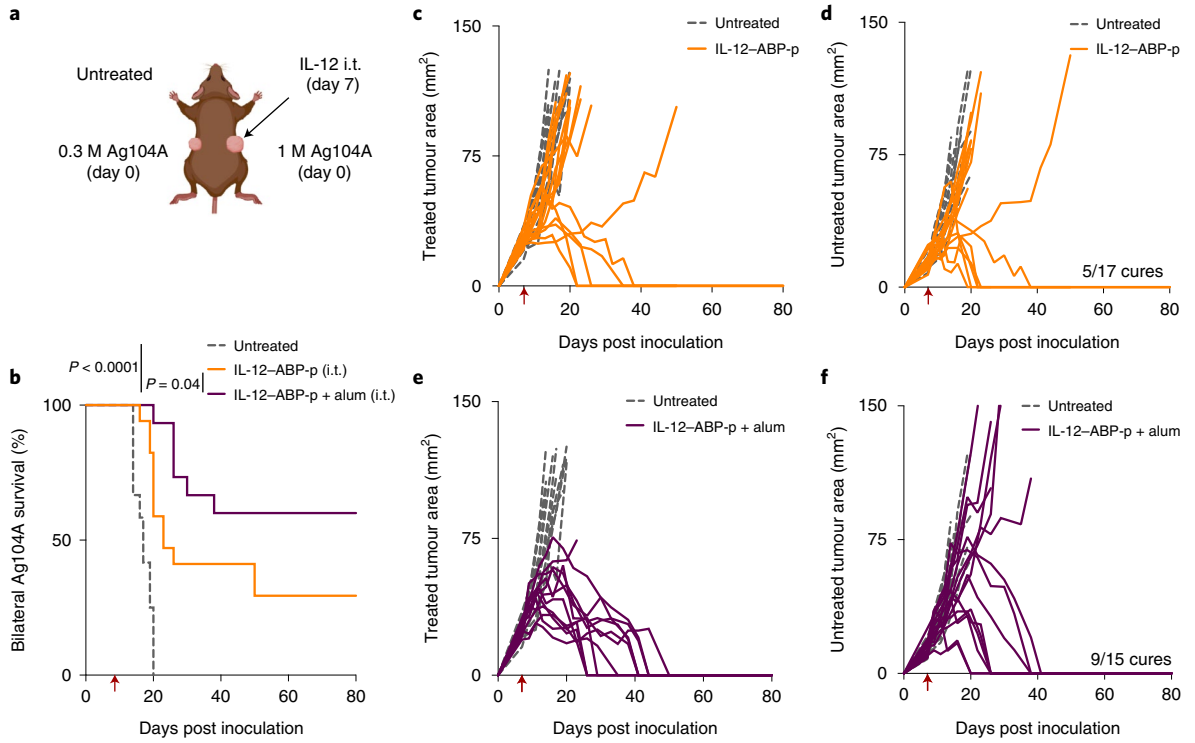

Fig. 4 | A single local dose of anchored IL-12 controls distal, untreated tumours. a–f, C3H-Hej mice (untreated $n = 10$ mice/group, IL-12–ABP-p intratumourally $n = 17$ mice/group and IL-12–ABP-p + alum intratumourally. $n = 15$ mice/group) were inoculated s.c. with 10^6 and 0.3×10^6 Ag104A cells on the right and left flanks, respectively. At day 7, the right flank tumour was treated intratumourally with 20 μg IL-12–ABP-p alone or mixed with 100 μg alum. Shown is the experimental setup (**a**), overall mouse survival (**b**) and individual tumour growth curves for treated (**c**,**e**) and untreated (**d**,**f**) tumours for mice treated with IL-12–ABP-p (**c**,**d**) or IL-12–ABP-p + alum (**e**,**f**). Red arrows indicate timing of i.t. treatments. ABP refers specifically to ABP10. *P* values were determined by the log-rank (Mantel–Cox) test (**b**) using GraphPad PRISM.

released from alum over ~2 weeks (Supplementary Fig. 2b). IL-12 anchoring on alum increased the size of alum crystal microaggregates in saline (Supplementary Fig. 2c), but the nanoscale morphology of alum nanorods appeared unchanged (Supplementary Fig. 2d,e). Further, the bioactivity of IL-12–ABP-p was similar to native single-chain IL-12 as measured by splenocyte activation (Fig. 1f) and HEK-Blue IL-12 reporter cell activation (Supplementary Fig. 2f,g). Interestingly, IL-12–ABP-p remained functional while adsorbed to alum particles, although with a several-fold reduction in half-maximal effective concentration (EC_{50}) (Fig. 1f and Supplementary Fig. 2h). The bioactivity of alum-bound IL-12–ABP-p was essentially constant even following multiple days of incubation in serum at 37 °C, indicating high in vitro stability for alum–cytokine complexes (Supplementary Fig. 2i). We also analysed in vitro alum binding and bioactivity of IL-2–ABP and IL-15sa–ABP fusion proteins. Similar to IL-12, when tagged with the phosphorylated ABP, these cytokines also showed enhanced retention on alum following serum exposure (Supplementary Fig. 2j,k). IL-2–ABP-p exhibited a four-fold loss in activity when bound to alum similar to IL-12–ABP-p, while IL-15sa–ABP-p showed no change in bioactivity when bound to alum (Supplementary Fig. 2l,m). Thus, ABP-fusion cytokines produced by in-cell phosphorylation exhibit stable alum binding and remain functional while immobilized on alum in vitro.

Alum-bound IL-12 safely persists in vivo after treatment. We next assessed the biodistribution and pharmacokinetics of alum-bound IL-12–ABP-p in vivo. We previously reported a strategy to stably label alum particles using an AlexaFluor 488 dye conjugated to a solid phase-synthesized poly-phosphoserine ($pSer_4$) peptide[31]. Alum was labelled using this approach and combined with IL-12–ABP-p labelled with AlexaFluor 568 dye. Immediately following i.t. injection in subcutaneously (s.c.) implanted B16F10 melanoma tumours, we observed that alum and phosphorylated protein were co-localized and distributed throughout the tumour bed (Fig. 2a). Measurement of IL-12 remaining in tumours 24, 72 or even 144 h later revealed a >400-fold greater retention of alum-tethered IL-12–ABP-p versus free IL-12–ABP-p (Fig. 2b). IVIS whole-animal fluorescence imaging of labelled alum-bound IL-12–ABP-p showed persistence of the cytokine at high levels in injected tumours for weeks after a single dosing, while signal from IL-12–ABP-p injected without alum was rapidly cleared (Fig. 2c,d and Supplementary Fig. 3a). Note that the high density of dye-labelled protein bound to alum leads to some fluorescence quenching at time zero[31], which is alleviated over the first few days as some cytokine is released, lowering the dye density and causing an artificial increase in signal over the first few days post injection. Intratumoural injection of free IL-12–ABP-p or alum mixed with non-phosphorylated IL-12 led to high levels of the cytokine in serum a few hours after treatment, while alum/IL-12–ABP-p injection led to IL-12 levels that were not statistically different than the baseline of untreated mice (Fig. 2e and Supplementary Fig. 3b).

IL-12 induces IFN-γ secretion by lymphocytes, which has been associated with toxicity in IL-12 clinical trials[35]. To assess the impact of altered IL-12 pharmacokinetics on safety, we established Ag104A fibrosarcoma flank tumours in C3H-Hej mice, which are known to better model human sensitivity to IL-12 than C57Bl/6 mice[35]. Unanchored IL-12 rapidly dispersed in the blood as observed in C57Bl/6 mice (Supplementary Fig. 3c). Intratumoural injection of free IL-12 or alum mixed with non-phosphorylated IL-12

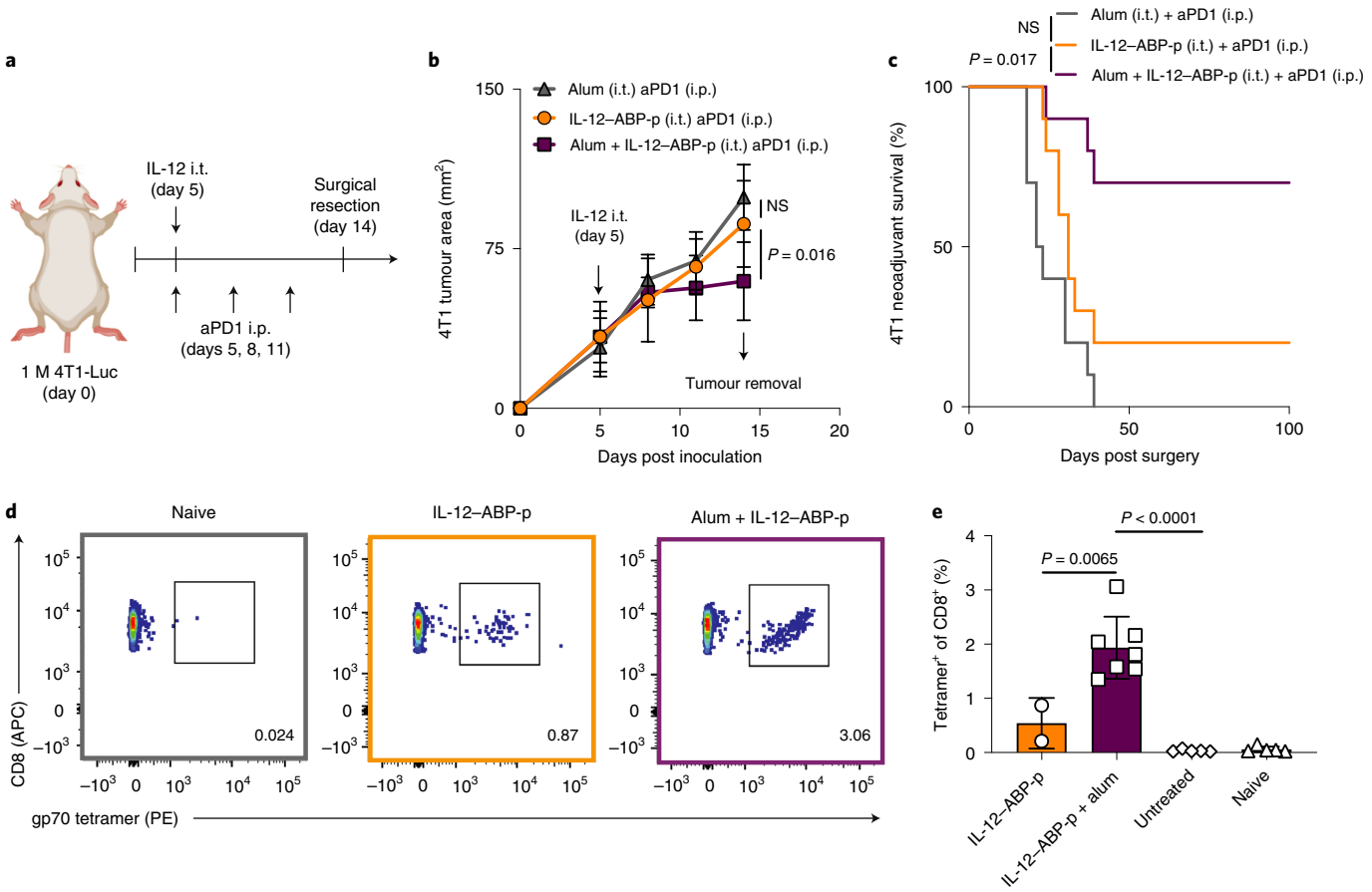

Fig. 5 | Neoadjuvant alum/IL-12 promotes systemic immunity in the orthotopic 4T1 breast cancer model. a–e, BALB/c mice ($n = 10$ mice for all groups) were inoculated with 0.5×10^6 4T1-Luc cells orthotopically in the mammary fat pad, and five days later, tumours were treated intratumourally with 20 μg IL-12–ABP-p, 100 μg alum or a combination of the two. Mice were also treated with 200 μg anti-PD1 i.p. on days 5, 8 and 11. On day 14, primary tumours were surgically removed. Shown is the experimental timeline (**a**), primary tumour growth (mean ± s.d., **b**) and overall survival (**c**). On day 56, peripheral blood of surviving mice (IL-12–ABP-p, $n = 2$ and IL-12–ABP-p/alum, $n = 7$), naïve mice ($n = 5$) and untreated animals bearing 14-day-old orthotopic 4T1 tumours ($n = 5$) was analysed by flow cytometry. Shown are representative flow plots (**d**) and quantification of gp70 tetramer⁺CD8⁺ T cells (**e**) in the peripheral blood. The numbers in the bottom right corner and the black squared area refer to the % gp70 tetramer+ out of all cells in the plot (**d**). The colors refer to the colors of the corresponding bars in (**e**). ABP refers specifically to ABP10. *P* values were determined by the log-rank (Mantel–Cox) test (**c**) and one-way (**e**) or two-way (**b**) ANOVA followed by Tukey's multiple comparison test using GraphPad PRISM. APC, allophycocyanin; PE, phycoerythrin.

led to animal weight loss, significant elevations in serum IFN-γ and alanine transaminase (ALT, indicating liver toxicity), and reduced albumin and total protein levels in blood after a single dose (Fig. 2f–h and Supplementary Fig. 3d–f). By contrast, i.t. injection of alum-anchored IL-12–ABP-p elicited significantly lower serum IFN-γ levels, prevented ALT levels from exceeding the normal clinical range, and left blood chemistry unaffected, correlating to no weight loss in treated animals (Fig. 2f–h and Supplementary Fig. 3d–f). Histopathological analysis of lungs from treated mice, however, did not reveal further toxicity (Supplementary Fig. 3g). Overall, anchoring of IL-12 to alum through the phosphorylated ABP led to efficient i.t. retention, substantially improving the systemic tolerability of this potent cytokine.

Anti-tumour efficacy is stronger with i.t. IL-12 retention. Dosing of alum-bound IL-12 intratumourally was not only safer but also much more effective. A single i.t. dose of IL-12–ABP-p + alum into large subcutaneous Ag104A tumours led to complete responses in 11 of 13 animals, while unanchored IL-12–ABP-p was only moderately effective and led to treatment-related mortality in 1 of 13 animals (Fig. 3a and Supplementary Fig. 4a).

While many cytokines have unacceptable toxicity when administered systemically, checkpoint blockade antibodies and antibodies against tumour cell surface antigens are better tolerated and are approved as systemic treatments. Thus, we also investigated the anti-tumour efficacy of combining a single i.t. alum/ABP–cytokine dose with systemic administration of antibodies modelling clinically relevant treatment combinations. We first treated mice bearing established B16F10 melanoma tumours intratumourally with a single dose of MSA–IL-2 accompanied by systemic administration of an antibody against tyrosinase-related protein 1 (anti-TYRP-1 or TA99). We previously reported that TA99 combined with MSA–IL-2 fused to the collagen-binding protein lumican leads to some curative responses in this model following multiple doses[28]. Alum-bound phosphorylated MSA–IL-2–ABP-p combined with TA99 regressed tumours and elicited complete responses in the majority of treated animals following a single dose (Fig. 3b and Supplementary Fig. 4b,e). By contrast, injection of MSA–IL-2–ABP-p in the absence of alum or administration of alum mixed with unphosphorylated MSA–IL-2 elicited little survival benefit over treatment with the TA99 alone, with no long-term survivors (Fig. 3b and Supplementary Fig. 4b–e). Moreover, a single injection

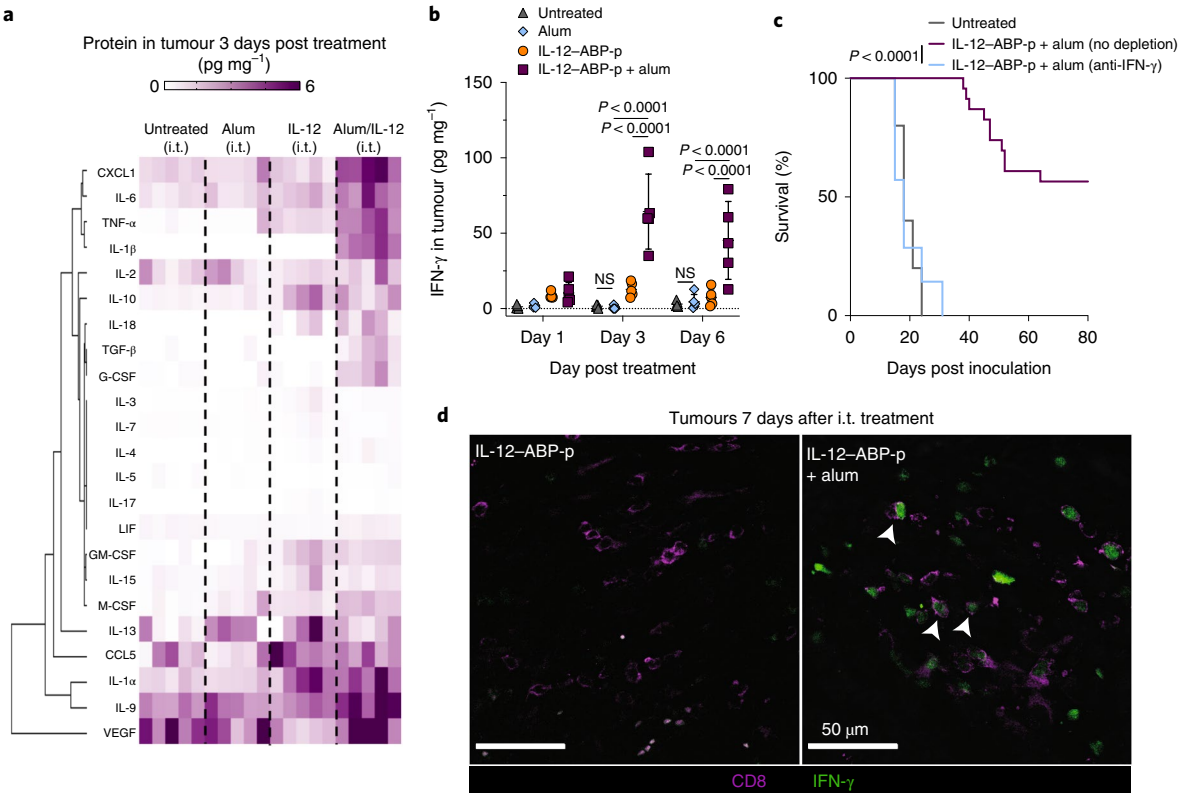

Fig. 6 | IFN-γ production is critical for alum-anchored IL-12-mediated tumour rejection. a,**b**, Mice were inoculated s.c. in the flank with 10^6 B16F10 tumour cells and treated on day 6 with no i.t. treatment ($n = 5$ mice per group), alum (100 μg) intratumourally, IL-12–ABP-p (20 μg) intratumourally or IL-12–ABP-p (20 μg) + alum (100 μg) intratumourally combined with systemic anti-PD1 (200 μg per dose) on days 6 and 9. Tumours were isolated and cytokine/chemokine levels quantified by Luminex 3 days post treatment (**a**), and IFN-γ amounts in tumours 1, 3 or 6 days after treatment were quantified by ELISA (mean ± s.d., **b**). **c**, Overall survival for mice bearing B16F10 tumours and treated as in **a** in the presence or absence of anti-IFN-γ starting 1 day before i.t. treatment and every 2 days thereafter (untreated $n = 10$ mice per group, treated $n = 23$ mice per group, and treated + anti-IFN-γ $n = 7$ mice per group). **d**, IFN-γ reporter mice bearing B16F10 tumours were treated as in **a** with AF405-labelled IL-12–ABP-p alone or combined with alum. Shown are representative histological tumour cross sections 7 days after treatment, with IFN-γ in green and CD8 in magenta ($n = 3$ mice per group; scale bars, 50 μm; white arrows point to IFN-γ$^+$CD8$^+$ T cells). ABP refers specifically to ABP10. *P* values were determined by the log-rank (Mantel–Cox) test (**c**) and two-way (**b**) ANOVA followed by Tukey's multiple comparison test using GraphPad PRISM.

of lumican–MSA–IL-2 in combination with TA99 was significantly less effective than alum-bound IL-2 (Fig. 3b and Supplementary Fig. 4d). The majority of mice that rejected their primary tumours also rejected cancer cells on rechallenge for the IL-2/alum/TA99 combination (Supplementary Fig. 4f).

We next tested i.t. IL-12 treatment in the same tumour model in combination with anti-PD1 therapy. Intratumoural alum/IL-12–ABP-p combined with systemic anti-PD1 elicited complete responses in 12 of 23 mice, while unanchored IL-12–ABP-p provided only a modest tumour growth delay and no long-term survival (Fig. 3c and Supplementary Fig. 4g). Notably, anti-PD1 played an important role in the high efficacy of the alum-anchored IL-12/checkpoint blockade combination (Supplementary Fig. 4h). In this study, we also assessed the immunogenicity of IL-12–ABP-p constructs: compared with the positive control of mice immunized with ovalbumin (OVA) mixed with alum, no detectable anti-drug antibody responses were detected by enzyme-linked immunosorbent assay (ELISA) (Supplementary Fig. 4i). In another syngeneic tumour model, the MC38 colon carcinoma, single shot alum/IL-12–ABP-p therapy elicited even stronger responses (9/10 complete responses) in combination with systemic anti-PD1, while IL-12–ABP-p in the absence of alum was substantially less potent (Fig. 3d and Supplementary Fig. 4j).

The ability of alum anchoring to block cytokine dissemination into the blood prompted us to next test combinations of alum-bound cytokines. Treatment of B16F10 tumours with a single i.t. dose of alum-tethered MSA–IL-2–ABP-p and IL-12–ABP-p accompanied by systemic anti-PD1 led to tumour eradication in nine of ten mice with no weight loss (Fig. 3e,f). By contrast, i.t. administration of this cytokine combination in the absence of alum led to pronounced weight loss and much poorer efficacy (Fig. 3e,f). In summary, by anchoring cytokines to alum via phosphorylation, both the safety and anti-tumour efficacy are enhanced in diverse tumour models, and clinically relevant combination treatments achieve high levels of therapeutic efficacy following a single i.t. injection.

Alum–cytokine treatment promotes control over distal lesions. The success of any i.t. therapy in the clinic will depend on its ability to promote systemic anti-tumour responses to control distal, untreated lesions and micro-metastases[16,36]. Therefore, we tested the ability of single-shot alum–IL-12 therapy to promote abscopal responses using two distinct models. First, we established Ag104A tumours on opposite flanks of mice and treated only one of the tumours with a single dose of alum with anchored IL-12–ABP-p (Fig. 4a). Even though IL-12 leakage into the blood was eliminated by alum binding, single-dose IL-12–ABP-p/alum exhibited greater efficacy than IL-12 alone, and elicited a systemic response that eliminated established distal untreated tumours in the absence of systemic checkpoint blockade therapy (Fig. 4b–f). Alum-anchored IL-12–ABP-p also significantly outperformed free IL-12–ABP-p in

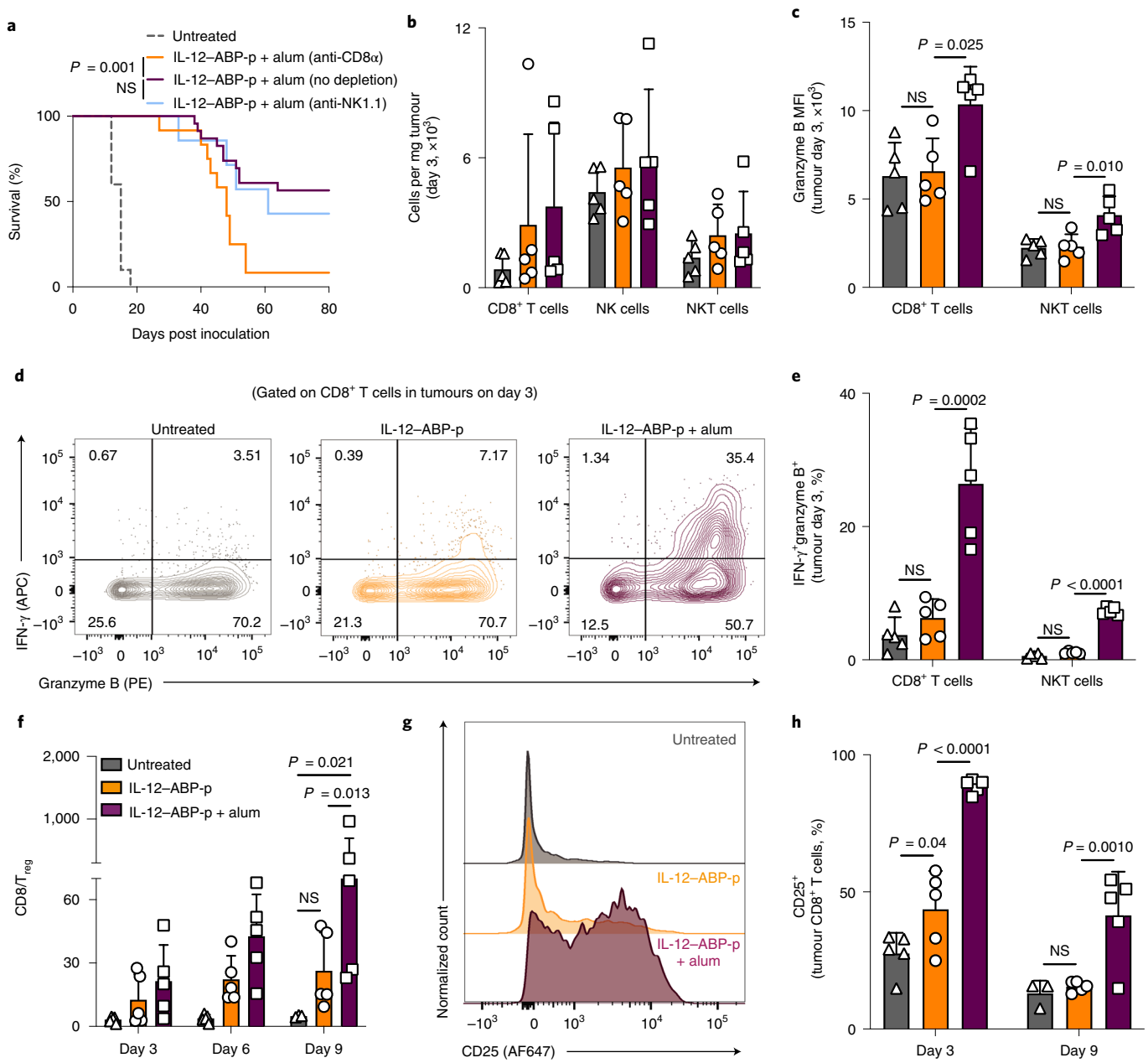

Fig. 7 | Single-dose alum/IL-12 therapy enhances i.t. T and NKT cell activity. a, Overall survival for mice bearing B16F10 tumours treated as in Fig. 3c that were also administered depleting antibodies starting 1 day before treatment and every 3 days thereafter (untreated $n = 10$ mice per group, treated $n = 23$ mice per group, treated + anti-CD8α $n = 12$ mice per group, and treated + anti-NK1.1 $n = 7$ mice per group). **b**–**h**, Mice bearing B16F10 tumours ($n = 5$ mice per group) were treated as in Fig. 6a. Tumours were analysed on days 3, 6 and 9 after treatment by flow cytometry. Shown are the quantification of tumour-infiltrating CD8⁺ T, NK and NKT cells (mean ± s.d., **b**), granzyme B geometric mean fluorescent intensity (MFI) (**c**), representative flow plots for i.t. CD8⁺ T cells (**d**) and enumeration (mean ± s.d.) of i.t. IFN-γ⁺granzyme B⁺ CD8⁺ T and NKT cells (**e**) on day 3. Numbers on the plots refer to the % cells in the quadrant out of all cells in the representative flow plots (**d**). **f**, Ratio of CD8⁺ T-cell counts to FoxP3⁺CD25⁺ T_{reg} cell counts over time (mean ± s.d.). **g**,**h**, Representative day 3 flow plots (**g**) and quantification (mean ± s.d., **h**) of CD25 expression by i.t. CD8⁺ T cells. ABP refers specifically to ABP10. *P* values were determined by the log-rank (Mantel–Cox) test (**a**) and one-way (**c**,**e**) or two-way (**f**,**h**) ANOVA followed by Tukey's multiple comparison test using GraphPad PRISM.

mice with bilateral B16F10 tumours in combination with systemic anti-PD-1(Supplementary Fig. 4k,l).

A second important clinical treatment scenario is neoadjuvant therapy. To assess the potential of alum-bound cytokines to be effective in this setting, we orthotopically implanted spontaneously metastatic 4T1 breast cancer cells in the mammary fat pad of BALB/c mice, and treated established tumours with a single dose of alum, IL-12–ABP-p or IL-12–ABP-p + alum, in combination with systemic anti-PD1. Nine days after treatment, we surgically resected the primary tumours and monitored the mice for survival (Fig. 5a). Alum-bound IL-12–ABP-p notably slowed primary tumour progression relative to treatment with alum alone or free IL-12–ABP-p (Fig. 5b). In this model, animals are susceptible to relapse due to micro-metastases in the lungs. The combination of alum-bound IL-12–ABP-p and anti-PD1 led to long-term survival of ~75% of animals, in contrast to minimal benefit achieved by alum/anti-PD1

or IL-12/anti-PD1 (Fig. 5c). To evaluate whether this supplementary survival was due to improved tumour-specific T-cell responses, we analysed the peripheral blood of all survivor mice for the frequency of CD8$^+$ T cells specific to gp70, an endogenous retroviral antigen expressed by 4T1 cells[37]. Impressively, a single dose of alum-anchored IL-12 promoted high gp70 tetramer$^+$ T-cell responses over both age-matched untreated mice bearing orthotopic 4T1 tumours and the few long-term survivors treated with free IL-12–ABP-p (Fig. 5d,e). Thus, a single dose of alum-anchored IL-12 elicits systemic immunity enabling control over non-injected distal tumours in multiple tumour models.

Alum/IL-12-induced IFN-γ drives early tumour regression. IL-12 can activate cells from both the innate and adaptive immune compartments either directly or indirectly via IFN-γ[10,22,38–40]. To determine the cellular and molecular effectors implicated in the context of persistent i.t. IL-12, we first carried out quantification of cytokines and chemokines generated in the TME of B16F10 tumours. Three days post treatment, alum/IL-12–ABP-p upregulated a battery of inflammatory effector proteins, including IL-6, TNF-α, IL-1β, CXCL9 and CXCL10 (Fig. 6a and Supplementary Fig. 5a,b). By this timepoint, IFN-γ production was increased fivefold over treatment with alum alone or IL-12–ABP-p alone, and was sustained for at least 6 days (Fig. 6b), indicating that high amounts of intratumourally retained IL-12 are still active at this timepoint. Although alum is known to activate the NLRP3 inflammasome[41], cytokine release in tumours and anti-tumour efficacy were unaffected in *Nlrp3*$^{-/-}$ mice (Supplementary Fig. 5c–g).

Successful checkpoint blockade therapy in mice relies on strong collaboration between T-cell-produced IFN-γ and dendritic cell (DC)-produced IL-12[38]. Here, treatment in the presence of an IFN-γ-neutralizing antibody entirely eliminated the efficacy of alum-anchored IL-12 with immediate loss of tumour control (Fig. 6c and Supplementary Fig. 6a). Thus, we asked what key cellular effectors drive IFN-γ expression in response to IL-12 (Supplementary Fig. 7). While IFN-γ production was upregulated in multiple cell types by alum-anchored IL-12, CD8$^+$ T cells and natural killer T (NKT) cells made up roughly 88% of the IFN-γ-producing cells in the treated tumour, and alum-bound cytokine substantially increased IFN-γ production by these two populations relative to IL-12 alone (Supplementary Fig. 6b–d). Immunohistochemical analysis of treated B16F10 tumours in IFN-γ reporter mice[38] revealed that alum–IL-12–ABP-p treatment but not free IL-12–ABP-p induced pockets of IFN-γ$^+$ CD8$^+$ T cells deep in tumour lesions (white arrows, Fig. 6d), and in some regions IFN-γ$^+$ CD8$^+$ T cells appeared to interact directly with fluorescently labelled IL-12–ABP-p 1 week after treatment (yellow arrows, Supplementary Fig. 6e). Antibody-mediated depletions revealed that CD8α$^+$ cells are critical to early tumour control and long-term immunity, while NK1.1$^+$ cells did not have a statistically significant impact on therapeutic efficacy (Fig. 7a and Supplementary Figs. 8a and 9).

While we found no significant difference in tumour immune cell infiltration 3 days after i.t. injection of free versus alum-anchored IL-12 (Fig. 7b and Supplementary Fig. 8b), alum-bound IL-12 induced a substantial IFN-γ$^+$granzyme B$^+$ CD8$^+$ T-cell population with upregulated granzyme expression by three days after treatment, and similar trends in CD4$^+$ T cells, NK cells and NKT cells (Fig. 7c–e and Supplementary Fig. 8c–e). Over time, alum/IL-12 established a much higher CD8-to-regulatory T cell (T_{reg}) ratio in the tumour over unanchored IL-12 (Fig. 7f), and these infiltrating CD8$^+$ T cells showed higher expression of CD25 and CD107a over treatment with free IL-12–ABP-p in the tumour as long as 9 days after treatment (Fig. 7g,h and Supplementary Fig. 8f). Thus, a single dose of alum-anchored IL-12 induced effector responses from innate (NK, NKT) and adaptive (CD8$^+$, CD4$^+$ T cells) immune cells, but CD8$^+$ T cells and IFN-γ are critical for ultimate tumour control.

Alum/IL-12 boosts antigen uptake in draining lymph node. Alum-bound IL-12 induced rapid upregulation of IFN-γ expression from tumour-infiltrating T cells early after treatment, but the observation of immunological memory (Supplementary Fig. 4f) and sustained tumour antigen-specific T-cell responses (Fig. 5d,e) suggested that ultimate disease control may involve priming of de novo T-cell responses. We treated established B16F10 tumours in *Batf3*$^{-/-}$ animals lacking cross-presenting DCs[42] that are crucial for priming T cells against tumour antigens, and long-term survival after i.t. therapy was significantly reduced in these mice (Fig. 8a). To track tumour antigen uptake by DCs, we treated B16F10 tumours expressing the stable fluorescent protein Zsgreen[43] and analysed draining lymph nodes (dLNs) by flow cytometry (Supplementary Fig. 10). CD103$^+$ cDC1s were previously reported to be critical antigen-carrying cells for T-cell priming in the B16F10 tumour model[43,44]. While the infiltration of DC and other myeloid cell populations remained relatively unchanged within treated tumours (Supplementary Fig. 11a,b), activated, antigen-loaded CD103$^+$ DCs steadily increased over time only in the dLNs of alum/IL-12–ABP-p-treated animals (Fig. 8b,c). Further, injection of free IL-12–ABP-p without alum led to only slight transient increases in CD86 and MHC-II expression, but alum-anchored IL-12–ABP-p maintained this upregulation of CD86 and MHC-II in dLN CD103$^+$ DCs even 6 days after treatment, moving a large proportion of these cells into a more persistent CD86^{hi}MHC-II^{hi} state (Fig. 8d and Supplementary Fig. 11c).

Antibody-mediated depletions show that CSF1R$^+$ macrophages and monocytes also impacted long-term survival, while Ly6G$^+$ neutrophils did not (Fig. 8e). While both anchored and unanchored IL-12–ABP-p upregulated MHC-II and CD86 in tumour-infiltrating monocytes (Supplementary Fig. 11d,e), alum-bound IL-12–ABP-p

Fig. 8 | Intratumourally persistent IL-12 promotes tumour antigen accumulation in activated dLN APCs. a, Overall survival for B16F10-bearing wild-type (WT) or *Batf3*$^{-/-}$ mice (untreated WT $n = 10$ mice per group, untreated *Batf3*$^{-/-}$ $n = 5$ mice per group, IL-12–ABP-p + alum WT $n = 23$ mice per group, and IL-12–ABP-p + alum *Batf3*$^{-/-}$ $n = 8$ mice per group) treated as in Fig. 3c with indicated proteins intratumourally and anti-PD1 i.p. every 3 days after. **b–d**, Mice bearing B16F10–Zsgreen tumours ($n = 5$–7 mice per group) were treated intratumourally as indicated and i.p. with anti-PD1 every 3 days after treatment. CD103$^+$ DCs in dLNs were analysed by flow cytometry 1, 3 or 6 days after treatment. Shown are representative day 6 flow plots (**b**) and quantification (mean ± s.d., **c**) for CD103$^+$ DCs positive for both Zsgreen and CD86 and proportion of MHC-II^{hi}CD86^{hi} CD103$^+$ DCs (mean ± s.d., **d**). Numbers on the plots refer to the % cells in the quadrant out of all cells in the representative flow plots (**b**). **e**, Overall survival for mice bearing B16F10 tumours treated as in Fig. 3c that were also administered depleting antibodies starting 1 day before treatment and every 3 days thereafter (untreated $n = 10$ mice per group, treated $n = 23$ mice per group, treated + anti-Ly6G $n = 7$ mice per group, treated + anti-CSF1R $n = 7$ mice per group). **f–h**, dLN monocytes were analysed as in **b–d**. Shown are representative day 3 flow plots (**f**), enumeration of Zsgreen$^+$CD86^{hi} monocytes over time (mean ± s.d., **g**) and enumeration of CD11c+ monocytes at day 6 (mean ± s.d., **h**). **i**, B16F10-bearing mice ($n = 5$) were treated intratumourally as in Fig. 3c with indicated combinations and i.p. with anti-PD1 every 3 days. At day 10 post treatment, splenocytes were isolated and stimulated with irradiated B16F10 cells in an IFN-γ ELISPOT assay. Shown is the number of spot-forming units (SFU) per 10^6 splenocytes plated per group (mean ± s.d.) and representative images of ELISPOT wells. ABP refers specifically to ABP10. *P* values were determined by the log-rank (Mantel–Cox) test (**a**,**e**) and one-way (**h**,**i**) or two-way (**c**,**d**,**g**) ANOVA followed by Tukey's multiple comparison test using GraphPad PRISM.

expanded a greater dLN-infiltrating MHC-II$^+$ and CD86$^+$Zsgreen$^+$ monocyte population in dLNs, which peaked 3 days post treatment (Fig. 8f,g and Supplementary Fig. 11f,g). IL-12–ABP-p + alum also promoted CD11c expression in dLN monocytes, suggesting their differentiation toward monocyte-derived DCs (Fig. 8h). Other DC and macrophage populations in the dLNs, particularly migratory CD11b$^+$ DCs and medullary chord macrophages, also had higher levels of CD86 and Zsgreen uptake over time after treatment with alum-bound IL-12–ABP-p (Supplementary Fig. 11h–j). Consistent with these shifts in antigen uptake in antigen presenting cells (APCs), an IFN-γ enzyme-linked immune absorbent spot (ELISPOT), performed on irradiated B16F10 cells cultured with splenocytes collected 10 days after i.t. treatment of B16F10 tumours revealed substantially higher tumour-specific responses in mice treated with alum/IL-12–ABP-p than those treated with IL-12–ABP-p alone (Fig. 8i). In summary, by tethering IL-12 to alum and improving its

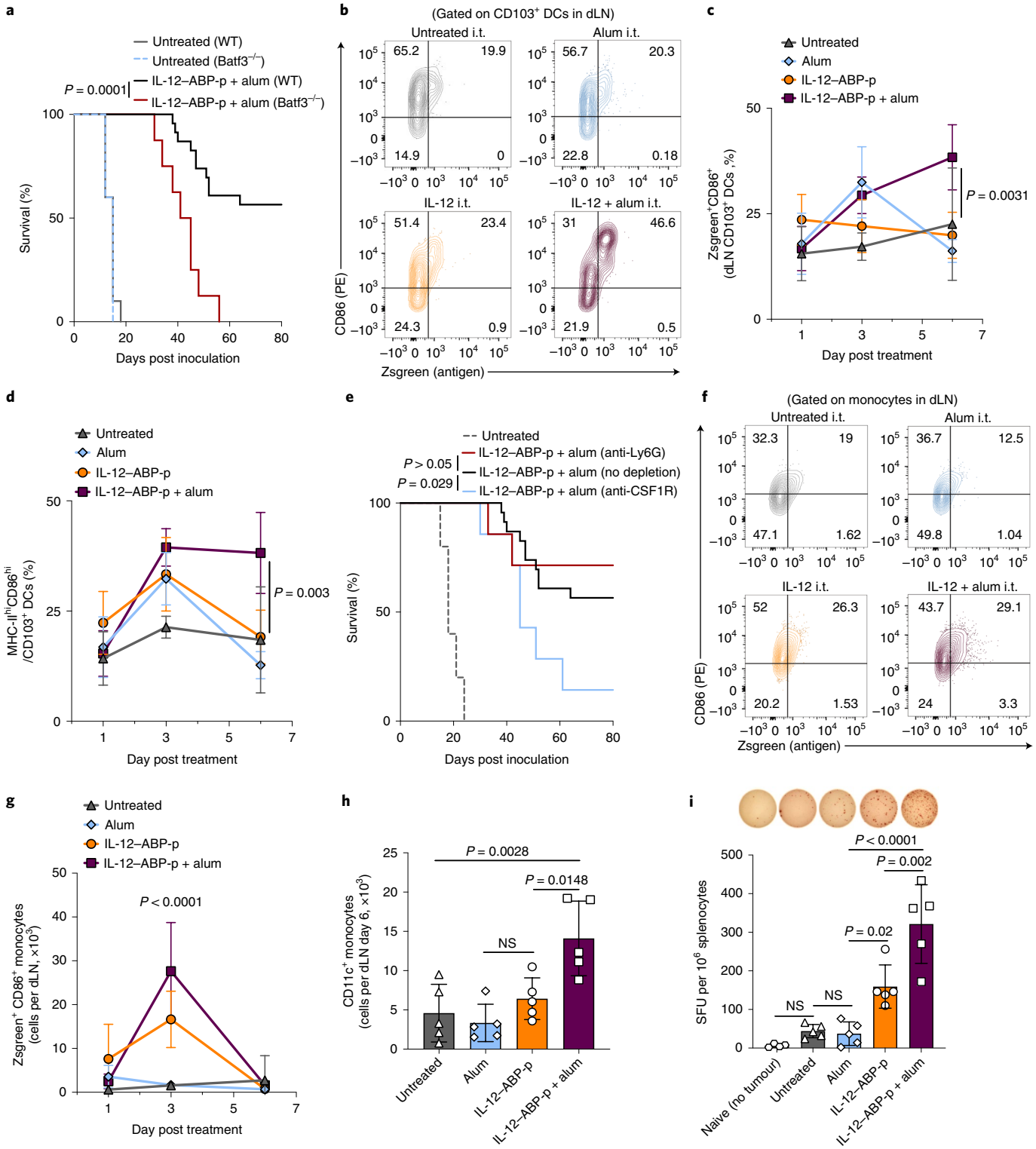

i.t. persistence following a single dose, several antigen-presenting myeloid cell types remain highly activated while presenting antigen in tumour dLNs and enhancing tumour-specific T-cell priming.

Discussion

Clinical translation of cytokine-based cancer immunotherapy has been challenging. So far, only IFNα and IL-2 have been approved by the US FDA for use in certain indications, and even those have fallen out of favour because of toxicity concerns[45]. IL-12 potently drives anti-tumour immunity in mouse models but has been found to have an unmanageably narrow therapeutic window in humans[22]. Here we report a modular approach for the local delivery of high-dose cytokine therapy with negligible toxicity. A single i.t. dose of alum-anchored cytokines enabled in situ vaccination, promoting durable local and systemic anti-tumour responses in several mouse cancer models.

Although other biomaterials such as injectable hydrogels[46–49], polymeric microspheres[50], Montanide ISA-51[51], mesoporous silica nanoparticles[52], microneedle patches[53,54] and other materials[22,55,56] have been explored for the local and sustained release of cytokines and chemokines in tumours, the FDA approval for use of these approaches in cancer remains a constant hurdle due to regulation, manufacturing and scalability challenges[57]. Further, precise engineering of the release rate of drugs to match their consumption rate in tumours has been extremely difficult, with clear evidence of drug leakage into the systemic circulation for most of these platforms[46,49]. For IL-12 in particular, there is considerable interest in the i.t. delivery of the IL-12 gene either via plasmid electroporation[58] or several viral and non-viral vectors[26,27]. However, this strategy also often results in the swift accumulation of IL-12 and IFN-γ in the blood[22]. By anchoring IL-12 to alum using phosphorylated peptide tags, we are able to dramatically limit such systemic dissemination, while maintaining high efficacy.

The number of clinical trials involving i.t. immunotherapy has increased swiftly over the past decade, and the oncolytic viral therapy talimogene laherparepvec (TVEC) became the first FDA-approved local immunotherapy in 2015. With innovations in interventional radiology and surgical techniques, essentially any lesion has become accessible for i.t. injections, making human i.t. immunotherapy a viable route for the administration of cancer drugs[59]. However, for lesions requiring surgery, treatments that can elicit prolonged immunostimulation following infrequent injections will be desirable, in combination with systemic dosing of approved therapies such as checkpoint blockade or tumour-targeting antibodies. In the single i.t. dose context, we show that alum-anchored IL-2 and IL-12 can greatly improve outcomes in both immunologically 'hot' (MC38) and 'cold' (B16F10) tumours in combination with checkpoint blockade or anti-tumour antibodies. We also see improved survival over collagen-anchored IL-2 in the single-dose setting. Strikingly, a single local dose of IL-12 also elicited systemic responses, delaying the growth of established untreated distal tumours in two different solid tumour models and greatly decreased lung metastases after neoadjuvant treatment of orthotopic 4T1 tumours, a model for triple-negative breast cancer.

Whereas enhancing i.t. residence of IL-12 led to the expected stimulation of T cells and NK cells to produce IFN-γ, we also observed notable activation of APC populations in dLNs, and increased tumour antigen accumulation in these cells. This effect could result from direct IL-12 signalling[40,60], IFN-γ-mediated reprogramming of DCs and monocytes[61,62] or an indirect outcome of tumour antigen and damage-associated molecular pattern release following cancer cell killing triggered by IFN-γ and granzyme B-producing T and NK cells. MHC-I upregulation by tumour cells after IFN-γ release is expected to promote cytolytic T-cell killing. Antibody-mediated neutralization experiments indicated that, while early tumour control may be entirely dependent on IFN-γ-driven immune responses, long-term tumour regression required both innate (cDC1, CSF1R+ monocytes and macrophages) and adaptive (CD8+ T cells) immune cells. The observed reprogramming of i.t. monocytes might also contribute to increased tumour-cell killing. Thus, by tethering IL-12 to alum for i.t. treatment, we not only restrict toxicity but also potentiate IL-12's pleiotropic therapeutic mechanisms of action.

Alum mixed with IL-12 was previously used to promote Th1 responses to sub-unit vaccines[63,64]. We used alum for the multi-day persistent delivery of cytokines to tumours. In the vaccine context, alum has been reported to improve humoral immunity by enabling sustained retention of antigen at injection sites, improving uptake by antigen-presenting cells, promoting necrosis and release of damage-associated molecular patterns at the injection site and signal through the NLRP3 inflammasome to elicit type-2-helper-T-cell-based antibody responses[32]. We found, however, that the NLRP3 inflammasome was not necessary for either inflammatory cytokine release or overall therapeutic efficacy for single-dose alum–IL-12 therapy. Some release of IL-6 and TNF-α does occur with i.t. treatments of just alum 1 day after treatment. This could be attributed to alum promoting necrosis in the tumour. However, this inflammation was only transient since i.t. injections of alum alone never led to substantial tumour control in any of the models we tested. Site-specific anchoring of proteins to solid surfaces can enhance stability and protect from endogenous, extracellular proteases. So, alum may also delay cytokine degradation in vivo and enhance the signalling period for cytokines[65].

In this study, we report the retention of alum-bound cytokines at injection sites for weeks after administration. Further, therapeutic efficacy appears to rely on strong activation driven by early IL-12 retention with enhanced IFN-γ secretion in the tumour lasting at least a week after treatment. Although delayed-type hypersensitivity to alum is rare and clinically manageable in humans[66], and we did not observe anti-ABP or anti-cytokine antibodies in treated animals, chronic inflammation due to long-term cytokine release at the sites of cured tumours could promote autoimmune reactions and granulomas[67]. Thus, it will be of interest in future work to define an optimal window for cytokine signalling and evaluate the long-term degradation, accessibility and bioactivity of the alum–cytokine depot. If there is active, accessible IL-12 months after treatment, alterations in the ABP designs such as the addition of a protease cleavage tag or a pH-responsive linker[68] could be made to ensure the removal of the cytokine after primary tumour cure.

The intracellular Fam20C phosphorylation method was developed with manufacturability and generalizability in mind[31]. For biomanufacturing generality and to take advantage of highly developed good manufacturing practice (GMP) cell expression platforms, we developed an in-cell phosphorylation strategy such that proteins are modified during secretion from mammalian cells. Stable cell lines expressing Fam20C could be next used for the transient transfection of any ABP-fusion protein of interest. Further, even proteins with internal S-x-E sites (IL-12p40 has two S-T-E sites) were only phosphorylated with the ABP present, indicating that the clustering of the motifs on one unstructured small peptide dominates phosphorylation. With some optimization in ABP design, linker sequence between ABP and target protein, and position of ABP within the protein, we have been able to apply this approach to antibodies, antibody–cytokine fusion proteins, other cytokines such as interferons, and other interleukins.

Finally, effective temporal programming may be critical to harnessing the true power of combination immunotherapy[69]. The customizability of the ABP approach may enable one to precisely control and tune release of proteins from alum in vivo and, eventually, programme timing such that a single shot of alum-anchored proteins would lead to release of distinct therapies at different times after treatment.

Methods

Cell lines and animals. Cell lines B16F10 (ATCC), HEK-Blue IL-12 (Invivogen), HEK293-F (Gibco), 4T1 (ATCC) and CTLL-2 (ATCC) cells were cultured following vendor instructions. 4T1-GFP-Luc (4T1-Luc) cells were generated by transfection of the 4T1 cell line with pGreenFire lentiviral vector (System Biosciences), and B16F10–Trp2 knock-out (KO) cells were generated as previously described by Moynihan et al.[8]. Ag104A, MC38 and B16F10-Zsgreen cells were a gift from H. Schreiber (University of Chicago), J. Schlom (National Cancer Institute) and R. Hynes (Massachusetts Institute of Technology (MIT)), respectively. 4T1 cells were cultured in Roswell Park Memorial Institute (RPMI) 1640 medium (ATCC) supplemented with 10% foetal bovine serum (FBS), 100 units ml^{-1} penicillin and 100 μg ml^{-1} streptomycin, while Ag104A, MC38 and B16F10-Zsgreen were all cultured in complete Dulbecco's Modified Eagle's Medium supplemented with 10% FBS, 100 units ml^{-1} penicillin and 100 μg ml^{-1} streptomycin. All cells were maintained at 37 °C and 5% CO_2, and all tested negative for mycoplasma.

Female C57BL/6 (Taconic, C57BL/6NTac), Balb/C (JAX, 000651), *Batf3*$^{-/-}$ (JAX, 013755), *Nlrp3*$^{-/-}$ (JAX, 021302), albino B6 (JAX, 000058), C3H/Hej (JAX, 000659) and IFN-γ reporter GREAT (JAX, 017581) mice at 6–10 weeks age were purchased and maintained in the animal facility at the MIT. All animal studies and procedures were carried out following federal, state and local guidelines under an institutional animal care and use committee-approved animal protocol by the Committee of Animal Care at MIT.

Cloning, protein purification and phosphorylation analysis. Genes for single-chain IL-12 and MSA–IL-2 proteins were cloned into the gWiz vector (Genlantis) as previously described[28]. Murine version of IL-15sa was designed based on the human clinical candidate ALT-803 by replacing the sushi domain of the human IL-15 receptor α and human IL-15 sequences by those from mouse. Chimeric (sushiIL-15Rα-IL-15) sequences were synthesized as gBlock gene fragments (Integrated DNA technologies) and cloned into the gWiz vector. The sequences for ABP10 were designed based on previously reported successfully phosphorylated peptides[33]. SEE was the most abundant naturally phosphorylated motif, and the flanking residues determined were those that were repeated atleast twice in the panel. All ABPs were ordered as gBlock gene fragments or single-stranded DNA primers (Integrated DNA technologies) that were then cloned into IL-12, MSA–IL-2 or IL-15sa containing gWiz vectors by In-Fusion (Takara Bio) such that all ABP-containing proteins would have poly-histidine (His) tags. Site-directed mutagenesis was done via simple mutations in primers followed by PCR. Human cDNA for Fam20C (Horizon, previously DharmaCon) was also cloned into gWiz with a terminal KDEL tag (without a His tag). All plasmids were transformed into Stellar Competent Cells (Takara Bio) and purified using the NucleoBond Xtra Maxi EF endotoxin-free maxi-prep kit (Takara Bio).

For protein production, plasmids were transiently transfected into HEK293-F cells (1 mg total DNA L^{-1} cell culture) via polyethylenimine (2 mg L^{-1} cell culture) using the Freestyle 293 Expression system (Gibco). For all co-transfections, target protein plasmid:Fam20C plasmid transfection mass ratio was restricted to 9:1. TA99 was purified using rProtein A Sepharose Fast Flow resin (Cytiva Life Sciences, formerly GE Healthcare) as described previously[8]. His-tagged proteins from cell culture supernatants were then purified using HisPur Ni-NTA metal affinity resin (Thermo Fisher Scientific). Monomeric phosphorylated proteins were further purified using custom anion exchange chromatography salt gradients (Supplementary Data Fig. 1) on HiTrap Q HP columns attached to an AKTA FPLC system (Cytiva Life Sciences, formerly GE Healthcare). Proteins were buffer exchanged into Tris-buffered saline (TBS, 1×, Sigma-Aldrich) using appropriate Amicon spin columns (Sigma-Aldrich). Purified proteins were confirmed to have low endotoxin levels (<0.1 EU per dose) by the Endosafe Nexgen-PTS system (Charles River) and validated for size by SDS–PAGE and phosphorylation by a malachite green assay (Pierce Phosphoprotein Phosphate Estimation Assay Kit, Thermo Fisher Scientific). Further validation of phosphorylation was done by western blot. Briefly, proteins were run on a NuPAGE gel in 2-(*N*-morpholino) ethanesulfonic acid, transferred onto a nitrocellulose membrane using the iBlot system (Invitrogen). The membrane was blocked by 0.5× Odyssey blocking buffer (LI-COR), and then stained with a rabbit anti-pSer antibody (Abcam, ab9332, 1:125) and anti-rabbit IR800 antibody (LI-COR, 1:10,000).

In vitro alum-binding and bioactivity assays. All alum used in the study was Alhydrogel purchased from Invivogen. Alum-binding assays were performed as described previously[31]. Briefly, proteins were conjugated to Alexa Fluor 647 (AF647) via NHS labelling (Invitrogen), mixed with alum with a mass ratio of 10:1 alum:protein unless otherwise noted in TBS and rotated at room temperature (r.t.) for 20 min to enable adsorption. Subsequently, the samples were centrifuged at 10,000*g* for 10 min to pellet alum, and the supernatant was aliquoted and replaced with 10% mouse serum-containing PBS. The tubes were then moved to a rotator at 37 °C. At indicated timepoints, the samples were removed and centrifuged, and the supernatant was replaced with free 10% mouse serum-containing PBS. All removed supernatants were analysed for fluorescence using a Tecan Infinite M200 Pro absorbance/fluorescence plate reader, and the results were normalized to samples that had no alum.

All bioactivity assays were performed in U-bottom plates to maximize alum–protein–cell interactions. For IL-12 bioactivity, two in vitro assays were used: HEK-Blue IL-12 reporter assay and ex vivo splenocyte stimulation assay. The HEK-Blue assay (Invivogen) was run according to manufacturer's instructions with 5:1 alum:IL-12 mass ratio. For serum stability assay, alum/IL-12 mixtures were incubated in TBS supplemented with 20% FBS for the indicated time before adding to cells. For the splenocyte assay, spleens were collected from C57BL/6 mice and processed into single-cell suspensions. Red blood cells were lysed with ACK lysing buffer (Gibco) and splenocytes plated in a 96-well plate at 500,000 cells per well. Then, IL-12, IL-12–ABP-p, IL-12–ABP-p + alum or just alum were added at indicated concentrations and incubated with splenocytes for 48 h at 37 °C. Supernatants were diluted 3× and analysed for IFN-γ via ELISA (Mouse IFNγ DuoSet ELISA, R&D Systems). Culture medium was RPMI supplemented with 10% FBS, 1% penicillin–streptomycin, 1× non-essential amino acids (Invitrogen), 1× sodium pyruvate (Invitrogen), 1× 2-mercaptoethanol (Invitrogen) and 10 ng ml^{-1} mouse IL-2. For IL-2 and IL-15 bioactivity, 10,000 CTLL-2 cells were plated in incomplete medium (no T-STIM w/ ConA) with indicated concentrations of recombinant MSA–IL-2 or IL-15 proteins with or without alum and incubated for 48 h at 37 °C. Mass ratio used was 2.5:1 and 5:1 alum:protein for MSA–IL-2 and IL-15, respectively. Cell viability was determined via the ATP-detecting CellTiter-Glo 2.0 assay (Promega) as per the manufacturer's instructions. Luminescence was measured using the Tecan plate reader with 0.25 s integration time.

Morphology and size characterization of alum/cytokine particles. Transmission electron microscopy was used to analyse morphology of particles. For this, 10 μL of pre-mixed alum/IL-12 or alum alone was dropped on 200 mesh copper grids coated with a continuous carbon film and dried at r.t. Grids were then mounted on a JEOL single tilt holder equipped in the JEOL 2100 FEG microscope. The microscope was operated at 200 kV and with a magnification in the range of ~10,000–60,000 for assessing particle size and distribution. All images were recorded on a Gatan 2k × 2k UltraScan CCD camera.

The size of alum-bound protein particles was assessed using a Horiba Partica LA-950V2 Laser Diffraction Particle Size Distribution Analyzer with a FractionCell Ultra-small Volume Solvent Resistant Cuvette.

Histopathology analysis. C3H/Hej mice ($n = 3$) were left untreated or treated s.c. with 20 μg IL-12–ABP-p alone or mixed with 100 μg alum. Three days after treatment, lungs and livers of the mice were collected and fixed in 10% formalin. The organs were embedded in paraffin, and blocks were cut into 4 μm sections followed by haematoxylin and eosin staining. The slides were imaged using the Aperio Digital Slide Scanning System (Leica). The slides were then blindly assessed for tissue damage, by the pathologist Dr R. Bronson.

IVIS. Albino B6 mice were inoculated with one million apigmented B16F10–Trp2 KO cells s.c. on the right flank. After the tumours became palpable (day 6), tumours were intratumourally treated with 30 μL of AF647-labelled proteins mixed with alum. For IL-12, 20 μg (~316 pmol) of protein (IL-12, IL-12–ABP, IL-12–ABP-p) was mixed with 100 μg alum in TBS and rotated in the dark at r.t. for 20 min before administration. After treatment, mice were imaged with the IVIS Spectrum imaging system (Perkin Elmer) under 0.5 s exposure epi-illumination fluorescence settings. Image analysis was done using Living Image (Caliper Life Sciences), and data were normalized to maximum radiance throughout the experiment per protein.

Tumour inoculation and i.t. therapy for subcutaneous flank models. For single-tumour efficacy experiments, 10^6 B16F10, Ag104A or MC38 cells in 50 μL sterile PBS were inoculated on the shaved right flank of mice (B6 for B16F10, MC38 and C3H for Ag104A). At day 6 after tumour inoculation for B16F10 or day 7 for MC38/Ag104A, tumours were treated intratumourally with a 30 μL injection. For all IL-12 treatments, 20 μg of IL-12–ABP-p was used (316 pmol) and the alum:protein mass ratio was 5:1 (20 μg IL-12:100 μg alum). On the other hand, IL-2 treatment was limited to 36 μg of MSA–IL-2–ABP-p (409 pmol, Fig. 3a) or 40 μg of MSA–IL-2–ABP-p (454 pmol, Fig. 3g), and the alum:protein mass ratio was 2.5:1. For all experiments, cytokines and alum were pre-mixed in TBS and rotated at r.t. for 20 min before administration. TA99 and aPD1 (clone 29F.1A12, BioXCell) were administered at 200 μg per dose in PBS intraperitoneally (i.p.) when indicated. Tumour area was measured by computing the product of the length and width of flank tumours, and mice were euthanized when the tumour area exceeded 100 mm^2 or if weight loss increased beyond 20%. For rechallenge experiments, 10^5 tumour cells were inoculated on the left flank of mice that rejected primary tumours.

For the Ag104A bilateral tumour model, one million Ag104A cells were inoculated on the right flank of C3H mice while 3×10^5 tumour cells were inoculated on the left flank on the same day. For the B16F10 bilateral tumour model, one million B16F10 cells were inoculated on the right flank of B6 mice while 5×10^5 cells were inoculated on the left flank 3 days after. Intratumoural treatments for both models occurred in the tumour on the right at day 6 for B16F10 and day 7 for Ag104A. Mice were euthanized when either tumour area exceeded 100 mm^2 or if weight loss increased beyond 20%.

IFN-γ ELISPOT. C57BL/6 mice ($n = 5$ animals per group) bearing 25 mm^2 B16F10 tumours (~day 6 after 10^6 cells were inoculated in the flank) were treated with no i.t. treatment, 100 μg alum intratumourally, 20 μg IL-12–ABP-p intratumourally or 20 μg IL-12–ABP-p + 100 μg IL-12–ABP-p along with 200 μg anti-PD1 i.p. on days 6, 9, 12 and 15. On day 16 (10 days after i.t. treatment), spleens were isolated from mice, mechanically digested through 70 μm nylon cell strainers to prepare single-cell suspensions in RPMI supplemented with 10% FBS, 1% penicillin–streptomycin, 1× non-essential amino acids (Invitrogen), 1× sodium pyruvate (Invitrogen) and 1× 2-mercaptoethanol (Invitrogen). Red blood cells were lysed in ACK Lysis Buffer (Gibco). On the same day, B16F10 cells (treated with 500 U ml^{-1} IFN-γ overnight) were subjected to 120 Gy radiation and trypsinized into a single-cell suspension in the same supplemented RPMI. Then, 25,000 irradiated B16F10 cells were mixed with 2.5×10^5 splenocytes per sample and seeded in a 96-well ELISPOT plate (BD Biosciences) that was pre-coated with IFN-γ capture antibody (BD Biosciences). Plates were wrapped in foil and cultured for 24 h in a 37 °C incubator, then developed according to the manufacturer's protocol. Plates were scanned using a CTL-ImmunoSpot Plate Reader, and data were analysed using CTL ImmunoSpot Software.

Depletion studies. Depletions of immune cells were done using antibodies against CD8α (clone 2.43, BioXCell 400 μg i.p. twice weekly), NK1.1 (clone PK136, BioXCell, 400 μg i.p. twice weekly), Ly6g (clone 1A8, BioXCell, 400 μg i.p. twice weekly) or CSF1R (clone AFS98, BioXCell, 300 μg i.p. every other day) as previously described[26]. Cytokine neutralization was done using intraperitoneal treatments with 200 μg of antibodies against IFN-γ (clone XMG1.2, BioXCell), IL-1β (clone B122, BioXCell) and IL-18 (clone YIGIF74-1G7, BioXCell) every other day. All depletion antibodies dosing was initiated 1 day before i.t. treatment and continued till at least 1 month after treatment.

Tumour inoculation, treatment and surgery for 4T1 orthotopic model. A total of 5×10^5 4T1-Luc tumour cells were inoculated into the fourth mammary fat pad of BALB/c mice, and palpable tumours 5 days after inoculation were treated intratumourally with 20 μg IL-12–ABP-p, 100 μg alum or a mixture of the two. Mice were also treated with 200 μg aPD1 i.p. on days 5, 8 and 11. Nine days after i.t. treatment (day 14), mice were anaesthetized with isoflurane and provided pre-operative subcutaneous sustained-release buprenorphine (1 mg kg^{-1}, ZooPharm) and meloxicam (5 mg kg^{-1}). The shaved surgical area was cleaned with alternating swabbing of betadine scrub and ethanol wipes. The primary tumour and draining inguinal lymph node were removed surgically using autoclaved surgical instruments (Braintree Scientific), and the wound was closed with surgical clips. Inguinal lymph nodes were removed due to primary tumours frequently growing around the node; therefore, the inguinal lymph node was removed in all mice. Meloxicam (5 mg kg^{-1}) was dosed every 24 h for 3 days post-operation. Mice were then monitored every other day and euthanized if signs of distress, >20% body weight loss, or poor body condition were observed.

ELISA, Luminex and blood chemistry analysis. To analyse anti-drug antibodies after treatment in mice, blood was collected by sub-mandibular bleeding from mice with long-term tumour rejection after treatment with IL-12–ABP-p + alum into Z-gel clotting tubes (Sarstedt). The tubes were centrifuged at 10,000*g* for 5 min, and separated serum was stored at −80 °C. Serum for control B6 mice was collected 3 weeks after subcutaneous treatment with 20 μg OVA (Sigma-Aldrich) adsorbed to 100 μg alum. MaxiSorp Immuno plates (Thermo Fisher) were coated with 2 μg ml^{-1} of OVA or IL-12–ABP-p in PBS at 4 °C for 2 days. This was followed by 2 h r.t. blocking with PBS + 1% bovine serum albumin. Subsequently, serial dilutions of collected serum in PBS + 1% bovine serum albumin was performed, and samples were transferred to the coated plates for another 2 h r.t. incubation. Plates were washed with PBS–Tween between every incubation step. Then, anti-mouse IgG–horseradish peroxidase antibody (Biolegend, 5,000×) was added to the wells for a 1 h r.t. incubation. Finally, the plates were developed for 20 min with 3,3′,5,5′-tetramethylbenzidine (Thermo Fisher Scientific), followed by the addition of concentrated sulfuric acid to stop the reaction. Absorbance was measured at A450 (background subtracted by A540) by the Tecan plate reader.

For cytokine/chemokine analysis of serum and tumour lysate, blood was collected at indicated times as described earlier. while tumours were collected and ground in tissue protein extraction reagent (T-PER, Thermo Fisher Scientific, cat. no. 78510) with 1% Halt protease and phosphatase inhibitors (Thermo Fisher Scientific, cat. no. 78442). The lysates were incubated with tissue at 4 °C for 30 min with rotation and then centrifuged to remove debris. Supernatant was subsequently filtered using Corning Costar SpinX columns before flash-freezing in liquid nitrogen. Amounts of IL-12 and IFN-γ in the samples were estimated by ELISA kits from Thermo Fisher Scientific (IL-12, cat. no. 88-7121-22) and R&D Systems (IFN-γ, cat. no. DY485-05) as per manufacturer instructions. Lysates were also sent to Eve technologies (for a 31-plex Luminex analysis) or analysed in-house using the 13-plex Mouse Macrophage/Microglia Legendplex Panel (Biolegend). Protein amounts (normalized by mass of tumour analysed) were clustered by Cluster 3.0 developed by M. Eisen at Stanford University, and the heatmap was generated by TreeView 3.0. Serum samples were sent to IDEXX Reference Laboratories for analysis of ALT, blood urea nitrogen, albumin and total protein.

Immunohistochemistry of alum-treated tumours. To stain for alum particles independently from ABP-fusion proteins, we relied on fluorophore-conjugated pSer peptides synthesized as described previously[31]. For Fig. 2a, B16F10 tumours were treated intratumourally with pre-mixed 20 μg AF568–IL-12–ABP-p, 0.4 nmol AF488–pSer4 and 100 μg alum, and treated tumours were removed 30 min after treatment. For Fig. 5d and Supplementary Data Fig. 6e, B16F10 tumours established in IFN-γ–YFP GREAT mice were treated intratumourally with pre-mixed 20 μg AF405–IL-12–ABP-p, 0.4 nmol Cy3–pSer4 and 100 μg alum, and tumours were removed 7 days after treatment. For both instances, tumours were fixed with 4% paraformaldehyde overnight, and washed and embedded in a 3 wt% low melting point agarose at 37 °C, which was then cooled and allowed to solidify on ice for 15 min. Using a vibratome (Leica VT1000S), 100 μm sections were prepared and suspended in ice-cold PBS before transferring into a blocking solution containing 10% goat serum, 0.2% Triton-X100 and 0.05% sodium azide overnight at 37 °C before staining. For Fig. 2a, sections were stained with AF647 TA99, while for sections from GREAT mice, staining was done with APC anti-mouse CD8α Ly 2 (clone CT-CD8a, Cedarlane). Antibodies were diluted 1:100 in blocking buffer overnight at 37 °C, followed by washes with 0.05% Tween-20 in PBS and mounted on a glass slide with ProLong Diamond antifade mounting medium (Thermo Fisher Scientific). Images were acquired using a Leica SP8 laser scanning confocal microscope with a 25× water objective or 63× oil objective. Images were processed with the Fiji software.

Antibodies, staining and FACS analysis. Antibodies to CD8α (53-6.7), CD103 (2E7), Ly6C (HK1.4), F4/80 (BM8), CD11b (M1/70), CD86 (GL1), MHC2 or I-A/I-E (M5/114.15.2), CD24 (30-F1), CD11c (N418), CCR7 (4B12), CD169 (3D6.112), Ly6G (1A8), CD3 (17A2), NKp46 (29A1.4), Ki67 (16A8), NK1.1 (PK136), Tim3 (RMT3-23), granzyme B (QA17A02), FoxP3 (MF14), CD44 (1M7), IFN-γ (XMG1.2), CD107a (1D4B), CD62L (MEL-14), CD25 (PC61) and TNF-α (MP6-XT22) were obtained from Biolegend. Antibodies to CD45 (30-F11), CD8α (53-6.7) and CD4 (GK1.5) were purchased from BD Biosciences. All antibodies were diluted 1:100. Gp70 tetramer (T-Select H-2L^d MuLV gp70 Tetramer-SPSYVYHQF-PE) was purchased from MBL. Tetramer staining was performed in buffer containing 50 nM dasatinib with 1:50 antibody dilution. Viability was assessed using Zombie Aqua and UV (Biolegend, 1:1,000) for tumour and dLN samples or using DAPI for tetramer staining of blood samples. Intracellular staining for FoxP3, Ki67, IFN-γ, TNF-α and granzyme B was performed using the FoxP3 Transcription Factor Buffer Set (eBioscience).

B16F10 tumours and dLNs were collected 1, 3, 6 or 9 days after i.t. treatment of day 8 tumours. Both were mechanically digested through 70 μm nylon cell strainers to prepare single-cell suspensions. Blood was collected by sub-mandibular bleeding into K2-EDTA tubes (Greiner-Bio), and red blood cells were lysed in ACK Lysis Buffer (Gibco). All samples were then resuspended in ice-cold PBS containing 1% (w/v) bovine serum albumin and 2 mM EDTA (fluorescence-activated cell sorting (FACS) buffer) with precision count beads (Biolegend, normalized to the weight of tissue per sample) before staining. For intracellular cytokine/granule staining of tumour and dLN infiltrating cells, digested tissue samples were resuspended in RPMI supplemented with 10% FBS, 1% penicillin-streptomycin, 1X non-essential amino acids (Invitrogen), 1× sodium pyruvate (Invitrogen), 1× 2-mercaptoethanol (Invitrogen) and 5 μg ml^{-1} brefeldin A (Sigma-Aldrich) for 4 h at 37 °C prior to staining. Cells were analysed using BD FACS LSR Fortessa, or BD FACS Symphony A3 flow cytometers. Data were analysed in FlowJo.

Statistics and reproducibility. Statistics were performed using Prism (GraphPad). Statistical methods were not used to determine sample size, but sample numbers were chosen based on estimates from pilot studies and published results, such that appropriate statistical tests would yield statistically significant results. For survival studies, log-rank (Mantel–Cox) tests were used. For FACS studies involving multiple timepoints, two-way analyses of variance (ANOVAs) followed by Tukey's multiple comparison tests were used, while one-way ANOVAs or Student's *t*-tests were used for other experiments. The sample size for in vitro analysis was three and for in vivo analysis as annotated in figure legends. The details of statistical analysis for figures and Supplementary figures are included in the source data files.

Reporting Summary. Further information on research design is available in the Nature Research Reporting Summary linked to this article.

Data availability

The main data supporting the results in this study are available within the paper and its Supplementary Information. Any data supporting the findings of this study are also available from the corresponding authors on reasonable request. Source data are provided with this paper.

Received: 3 July 2021; Accepted: 5 November 2021;
Published online: 10 January 2022

References

1. Wolchok, J. D. et al. Overall survival with combined nivolumab and ipilimumab in advanced melanoma. *N. Engl. J. Med.* **377**, 1345–1356 (2017).
2. Ansell, S. M. et al. PD-1 blockade with nivolumab in relapsed or refractory Hodgkin's lymphoma. *N. Engl. J. Med.* **372**, 311–319 (2015).
3. Brahmer, J. et al. Nivolumab versus docetaxel in advanced squamous-cell non-small-cell lung cancer. *N. Engl. J. Med.* **373**, 123–135 (2015).
4. Bellmunt, J. et al. Pembrolizumab as second-line therapy for advanced urothelial carcinoma. *N. Engl. J. Med.* **376**, 1015–1026 (2017).
5. Yi, M. et al. Biomarkers for predicting efficacy of PD-1/PD-L1 inhibitors. *Mol. Cancer* **17**, 129 (2018).
6. Anderson, K. G., Stromnes, I. M. & Greenberg, P. D. Obstacles posed by the tumour microenvironment to T cell activity: a case for synergistic therapies. *Cancer Cell* **31**, 311–325 (2017).
7. Smyth, M. J., Ngiow, S. F., Ribas, A. & Teng, M. W. L. Combination cancer immunotherapies tailored to the tumour microenvironment. *Nat. Rev. Clin. Oncol.* **13**, 143–158 (2016).
8. Moynihan, K. D. et al. Eradication of large established tumours in mice by combination immunotherapy that engages innate and adaptive immune responses. *Nat. Med.* **22**, 1402–1410 (2016).
9. Milling, L., Zhang, Y. & Irvine, D. J. Delivering safer immunotherapies for cancer. *Adv. Drug Deliv. Rev.* **114**, 79–101 (2017).
10. Lasek, W., Zagożdżon, R. & Jakobisiak, M. Interleukin 12: still a promising candidate for tumour immunotherapy? *Cancer Immunol. Immunother.* **63**, 419–435 (2014).
11. Kirchner, G. I. et al. Pharmacokinetics of recombinant human interleukin-2 in advanced renal cell carcinoma patients following subcutaneous application. *Br. J. Clin. Pharmacol.* **46**, 5–10 (1998).
12. June, C. H., Warshauer, J. T. & Bluestone, J. A. Is autoimmunity the Achilles' heel of cancer immunotherapy? *Nat. Med.* **23**, 540–547 (2017).
13. Leonard, J. P. et al. Effects of single-dose interleukin-12 exposure on interleukin-12-associated toxicity and interferon-γ production *Blood* **90**, 2541–2548 (1997).
14. Atkins, M. B. et al. Phase I evaluation of intravenous recombinant human interleukin 12 in patients with advanced malignancies. *Clin. Cancer Res.* **3**, 409–417 (1997).
15. Melero, I. et al. Intratumoural administration and tumour tissue targeting of cancer immunotherapies. *Nat. Rev. Clin. Oncol.* https://doi.org/10.1038/s41571-021-00507-y (2021).
16. Aznar, M. A. et al. Intratumoural delivery of immunotherapy—act locally, think globally. *J. Immunol.* **198**, 31–39 (2017).
17. Marabelle, A., Kohrt, H., Caux, C. & Levy, R. Intratumoural immunization: a new paradigm for cancer therapy. *Clin. Cancer Res.* **20**, 1747–1756 (2014).
18. Brody, J. D. et al. In situ vaccination with a TLR9 agonist induces systemic lymphoma regression: a phase I/II study. *J. Clin. Oncol.* **28**, 4324–4332 (2010).
19. Posch, C. et al. Low-dose inhalation of interleukin-2 bio-chemotherapy for the treatment of pulmonary metastases in melanoma patients. *Br. J. Cancer* **110**, 1427–1432 (2014).
20. van Herpen, C. M. L. et al. Intratumoural rhIL-12 administration in head and neck squamous cell carcinoma patients induces B cell activation. *Int. J. Cancer* **123**, 2354–2361 (2008).
21. Pfreundschuh, M. G. et al. Phase I study of intratumoural application of recombinant human tumour necrosis factor. *Eur. J. Cancer Clin. Oncol.* **25**, 379–388 (1989).
22. Nguyen, K. G. et al. Localized interleukin-12 for cancer immunotherapy. *Front. Immunol.* **11**, 575597 (2020).
23. Younes, A. et al. Phase II clinical trial of interleukin-12 in patients with relapsed and refractory non-Hodgkin's lymphoma and Hodgkin's disease. *Clin. Cancer Res.* **10**, 5432–5438 (2004).
24. Little, R. F. et al. Activity of subcutaneous interleukin-12 in AIDS-related Kaposi sarcoma. *Blood* **107**, 4650–4657 (2006).
25. Car, B. D., Eng, V. M., Lipman, J. M., & Anderson, T. D. The toxicology of interleukin-12: a review. *Toxicol. Pathol.* **27**, 58–63 (1999).
26. Li, Y. et al. Multifunctional oncolytic nanoparticles deliver self-replicating IL-12 RNA to eliminate established tumours and prime systemic immunity. *Nat. Cancer* **1**, 882–893 (2020).
27. Chiocca, E. A. et al. Regulatable interleukin-12 gene therapy in patients with recurrent high-grade glioma: results of a phase 1 trial. *Sci. Transl. Med.* **11**, 505 (2019).
28. Momin, N. et al. Anchoring of intratumourally administered cytokines to collagen safely potentiates systemic cancer immunotherapy. *Sci. Transl. Med.* **11**, eaaw2614 (2019).
29. Flarend, R. E. et al. In vivo absorption of aluminium-containing vaccine adjuvants using 26Al. *Vaccine* **15**, 1314–1318 (1997).
30. Morefield, G. L. et al. Effect of phosphorylation of ovalbumin on adsorption by aluminum-containing adjuvants and elution upon exposure to interstitial fluid. *Vaccine* **23**, 1502–1506 (2005).
31. Moyer, T. J. et al. Engineered immunogen binding to alum adjuvant enhances humoral immunity. *Nat. Med.* **26**, 430–440 (2020).
32. Hogenesch, H., O'Hagan, D. T. & Fox, C. B. Optimizing the utilization of aluminum adjuvants in vaccines: you might just get what you want. *npj Vaccines* **3**, 51 (2018).
33. Tagliabracci, V. S. et al. A single kinase generates the majority of the secreted phosphoproteome. *Cell* **161**, 1619–1632 (2015).
34. Tagliabracci, V. S. et al. Secreted kinase phosphorylates extracellular proteins that regulate biomineralization. *Science* **336**, 1150–1153 (2012).
35. Leonard, J. P. et al. Effects of single-dose interleukin-12 exposure on interleukin-12-associated toxicity and interferon-g production. http://ashpublications.org/blood/article-pdf/90/7/2541/1415768/2541.pdf
36. Marabelle, A., Tselikas, L., de Baere, T. & Houot, R. Intratumoural immunotherapy: using the tumour as the remedy. *Ann. Oncol.* **28**, xii33–xii43 (2017).
37. Scrimieri, F. et al. Murine leukemia virus envelope gp70 is a shared biomarker for the high-sensitivity quantification of murine tumour burden. *Oncoimmunology* **2**, e26889 (2013).
38. Garris, C. S. et al. Successful anti-PD-1 cancer immunotherapy requires T cell–dendritic cell crosstalk involving the cytokines IFN-γ and IL-12. *Immunity* **49**, 1148–1161.e7 (2018).
39. Fallarino, F., Ashikari, A., Boon, T. & Gajewski, T. F. Antigen-specific regression of established tumours induced by active immunization with irradiated IL-12-but not B7-1-transfected tumour cells. *Int. Immunol.* **9**, 1259–1269 (1997).
40. Kerkar, S. P. et al. IL-12 triggers a programmatic change in dysfunctional myeloid-derived cells within mouse tumours. *J. Clin. Investig.* **121**, 4746–4757 (2011).
41. Eisenbarth, S. C., Colegio, O. R., O'Connor, W., Sutterwala, F. S. & Flavell, R. A. Crucial role for the Nalp3 inflammasome in the immunostimulatory properties of aluminium adjuvants. *Nature* **453**, 1122–1126 (2008).
42. Spranger, S., Dai, D., Horton, B. & Gajewski, T. F. Tumour-residing Batf3 dendritic cells are required for effector T cell trafficking and adoptive T cell therapy. *Cancer Cell* **31**, 711–723.e4 (2017).
43. Roberts, E. W. et al. Critical role for CD103(+)/CD141(+) dendritic cells bearing CCR7 for tumour antigen trafficking and priming of T cell immunity in melanoma. *Cancer Cell* **30**, 324–336 (2016).
44. Broz, M. L. et al. Dissecting the tumour myeloid compartment reveals rare activating antigen-presenting cells critical for T cell immunity. *Cancer Cell* **26**, 638–652 (2014).
45. Riley, R. S., June, C. H., Langer, R. & Mitchell, M. J. Delivery technologies for cancer immunotherapy. *Nat. Rev. Drug Discov.* **18**, 175–196 (2019).
46. Zaharoff, D. A., Hance, K. W., Rogers, C. J., Schlom, J. & Greiner, J. W. Intratumoural immunotherapy of established solid tumours with chitosan/IL-12. *J. Immunother.* **33**, 697–705 (2010).
47. Wang, C. et al. In situ formed reactive oxygen species-responsive scaffold with gemcitabine and checkpoint inhibitor for combination therapy. *Sci. Transl. Med.* **10**, 429 (2018).
48. Park, C. G. et al. Extended release of perioperative immunotherapy prevents tumour recurrence and eliminates metastases. *Sci. Transl. Med.* **10**, 433 (2018).
49. Hori, Y., Stern, P. J., Hynes, R. O. & Irvine, D. J. Engulfing tumours with synthetic extracellular matrices for cancer immunotherapy. *Biomaterials* **30**, 6757–6767 (2009).
50. Rahimian, S. et al. Polymeric microparticles for sustained and local delivery of antiCD40 and antiCTLA-4 in immunotherapy of cancer. *Biomaterials* **61**, 33–40 (2015).
51. Fransen, M. F., Sluijter, M., Morreau, H., Arens, R. & Melief, C. J. M. Local activation of CD8 T cells and systemic tumour eradication without toxicity via slow release and local delivery of agonistic CD40 antibody. *Clin. Cancer Res.* **17**, 2270–2280 (2011).
52. Paulson, J. A. et al. A facile approach to enhance antigen response for personalized cancer vaccination. *Nat. Mater.* **17**, 528–534 (2018).
53. Makvandi, P. et al. Stimuli-responsive transdermal microneedle patches. *Mater. Today* https://doi.org/10.1016/J.MATTOD.2021.03.012 (2021).
54. Wang, C. et al. Enhanced cancer immunotherapy by microneedle patch-assisted delivery of anti-PD1 antibody. *Nano Lett.* https://doi.org/10.1021/acs.nanolett.5b05030 (2016).
55. Yang, C., Blum, N. T., Lin, J., Qu, J. & Huang, P. Biomaterial scaffold-based local drug delivery systems for cancer immunotherapy. *Sci. Bull.* **65**, 1489–1504 (2020).
56. Zhao, Z. et al. Delivery strategies of cancer immunotherapy: recent advances and future perspectives. *J. Hematol. Oncol.* **12**, 126 (2019).
57. Xue, K. et al. Hydrogels as emerging materials for translational biomedicine. *Adv. Ther.* **2**, 1800088 (2019).
58. Burkart, C. et al. Improving therapeutic efficacy of IL-12 intratumoural gene electrotransfer through novel plasmid design and modified parameters. *Gene Ther.* **25**, 93–103 (2018).
59. Champiat, S. et al. Intratumoural immunotherapy: from trial design to clinical practice. *Clin. Cancer Res.* **27**, 665–679 (2021).
60. Nakahara, T. et al. Engagement of human monocyte-derived dendritic cells into interleukin (IL)-12 producers by IL-1β + interferon (IFN)-γ. *Clin. Exp. Immunol.* **139**, 476–482 (2005).

61. Kerkar, S. P. et al. Collapse of the tumour stroma is triggered by IL-12 induction of Fas. *Mol. Ther.* **21**, 1369–1377 (2013).
62. Goldszmid, R. S. et al. NK cell-derived interferon-γ orchestrates cellular dynamics and the differentiation of monocytes into dendritic cells at the site of infection. *Immunity* **36**, 1047–1059 (2012).
63. Hamid, O. et al. Alum with interleukin-12 augments immunity to a melanoma peptide vaccine: correlation with time to relapse in patients with resected high-risk disease. *Clin. Cancer Res.* **13**, 215–222 (2007).
64. Kenney, R. T. et al. Protective immunity using recombinant human IL-12 and alum as adjuvants in a primate model of cutaneous leishmaniasis. *J. Immunol.* **163**, 4481-4488 (1999).
65. Klibanov, A. M. Enzyme stabilization by immobilization. *Anal. Biochem.* **93**, 1–25 (1979).
66. Lauren, C. T. et al. Case report of subcutaneous nodules and sterile abscesses due to delayed type hypersensitivity to aluminum-containing vaccines. *Pediatrics* **138**, 4 (2016).
67. Caspi, R. R. Immunotherapy of autoimmunity and cancer: the penalty for success. *Nat. Rev. Immunol.* **8**, 970–976 (2008).
68. Dudani, J. S., Warren, A. D. & Bhatia, S. N. Harnessing protease activity to improve cancer care. *Annu. Rev. Cancer Biol.* **2**, 353–376 (2018).
69. Rothschilds, A. M. & Dane Wittrup, K. What, why, where, and when: bringing timing to immuno-oncology. *Trends Immunol.* **40**, 12–21 (2019).

Acknowledgements

Y.A. is partially supported by a graduate fellowship from the Ludwig Center at MIT's Koch Institute. D.J.I. is an investigator at the Howard Hughes Medical Institute. This work was supported by the Marble Center for Nanomedicine, the Ragon Institute of MGH, MIT and Harvard, and by the Koch Institute Support (core) Grant P30-CA14051 from the National Cancer Institute. L.E.M. and E.A.L. are supported by the NIGMS Biotechnology Training Grant T32GM833430, while L.S., A.S., E.A.L. and A.T. are supported by the NSF Graduate Research Fellowship Program. L.E.M. is also supported by Siebel Scholarship, L.S. is supported by the UCEM scholarship from the Alfred P. Sloan Foundation and A.T. is supported by the Paul & Daisy Soros Fellowship. We thank the Koch Institute Swanson Biotechnology Center for technical support, specifically the pre-clinical modelling, imaging and testing core facility, microscopy facility, histology facility, nanotechnology materials and the flow cytometry facility. We also thank H. Schreiber, R. Hynes and J. Scholm for critical reagents and all past and present members of Wittrup and Irvine laboratories for productive discussions and feedback regarding experiments and the manuscript. Figures 4a and 5a were created with BioRender.com.

Author contributions

Y.A., K.D.W. and D.J.I. conceived of the study and wrote the manuscript. Y.A. designed the experiments and analysed data. Y.A., L.E.M., J.Y.H.C., L.S., A.S., E.A.L., A.T. and J.S. performed the experiments and data analysis. K.A.R. assisted with the Horiba experiment, and K.N. performed the transmission electron microscopy imaging. K.A.R. and T.J.M. provided the AF488-pSer4 peptide, and M.D.M provided the plasmid for murine IL-15sa.

Competing interests

Y.A., D.J.I., K.D.W. and T.J.M. are named as inventors in patent applications filed by MIT related to the data presented in this work (US20200405950A1). K.D.W. and D.J.I. are co-founders of Ankyra Therapeutics, which has licensed rights to the MIT intellectual property mentioned above.

Additional information

Supplementary information The online version contains supplementary material available at https://doi.org/10.1038/s41551-021-00831-9.

Correspondence and requests for materials should be addressed to Darrell J. Irvine or K. Dane Wittrup.

Peer review information *Nature Biomedical Engineering* thanks Zhen Gu and the other, anonymous, reviewer(s) for their contribution to the peer review of this work. Peer reviewer reports are available.

Reprints and permissions information is available at www.nature.com/reprints.

Publisher's note Springer Nature remains neutral with regard to jurisdictional claims in published maps and institutional affiliations.

nature research

Corresponding author(s): K. Dane Wittrup, Darrell J. Irvine

Last updated by author(s): October 8, 2021

Reporting Summary

Nature Research wishes to improve the reproducibility of the work that we publish. This form provides structure for consistency and transparency in reporting. For further information on Nature Research policies, see our Editorial Policies and the Editorial Policy Checklist.

Statistics

For all statistical analyses, confirm that the following items are present in the figure legend, table legend, main text, or Methods section.

n/a	Confirmed
☐	☒ The exact sample size (*n*) for each experimental group/condition, given as a discrete number and unit of measurement
☐	☒ A statement on whether measurements were taken from distinct samples or whether the same sample was measured repeatedly
☐	☒ The statistical test(s) used AND whether they are one- or two-sided *Only common tests should be described solely by name; describe more complex techniques in the Methods section.*
☒	☐ A description of all covariates tested
☐	☒ A description of any assumptions or corrections, such as tests of normality and adjustment for multiple comparisons
☐	☒ A full description of the statistical parameters including central tendency (e.g. means) or other basic estimates (e.g. regression coefficient) AND variation (e.g. standard deviation) or associated estimates of uncertainty (e.g. confidence intervals)
☐	☒ For null hypothesis testing, the test statistic (e.g. *F*, *t*, *r*) with confidence intervals, effect sizes, degrees of freedom and *P* value noted *Give P values as exact values whenever suitable.*
☒	☐ For Bayesian analysis, information on the choice of priors and Markov chain Monte Carlo settings
☒	☐ For hierarchical and complex designs, identification of the appropriate level for tests and full reporting of outcomes
☒	☐ Estimates of effect sizes (e.g. Cohen's *d*, Pearson's *r*), indicating how they were calculated

Our web collection on statistics for biologists contains articles on many of the points above.

Software and code

Policy information about availability of computer code

Data collection	FACS data were obtained using the BD FACSDiva software. ELISA plates and plate-based fluorescent/absorbance experiments were measured using the Tecan Infinite M200 Pro absorbance/fluorescence plate reader and software. ELISPOT measurements were taken using the CTL Immunospot Analyzer and associated software. Western Blot analysis was made using a LI-COR ODyssey reader and LI-COR imaging software. Confocal images were taken on a Leica SP8 laser scanning confocal microscope and associated software. IVIS data were collected on the IVIS Spectrum In Vivo Imaging system. TEM images were collected using the JEOL 2100 FEG microscope, whereas particle size was collected with a Horiba Partica LA-950V2 Laser Diffraction Particle Size Distribution Analyzer.
Data analysis	FlowJo 10.7.1 was used for the analysis of FACS data. GraphPad Prism 9.1.2 was used for plotting and statistical analysis. Cluster 3.0 was used for hierarchical clustering of tumour cytokine/chemokine data. Fiji (Image J v2.1.0) was used for histology image analysis. Excel, Word and Powerpoint from Microsoft Office (version 16.49) were used to draft the manuscript. IVIS data were analysed using Living Image v4.5.

For manuscripts utilizing custom algorithms or software that are central to the research but not yet described in published literature, software must be made available to editors and reviewers. We strongly encourage code deposition in a community repository (e.g. GitHub). See the Nature Research guidelines for submitting code & software for further information.

Data

Policy information about availability of data

All manuscripts must include a data availability statement. This statement should provide the following information, where applicable:

- Accession codes, unique identifiers, or web links for publicly available datasets
- A list of figures that have associated raw data
- A description of any restrictions on data availability

The main data supporting the results in this study are available within the paper and its Supplementary Information. Source data for the figures are provided with this paper. Any data supporting the findings of this study are also available from the corresponding authors on reasonable request.

Field-specific reporting

Please select the one below that is the best fit for your research. If you are not sure, read the appropriate sections before making your selection.

☒ Life sciences ☐ Behavioural & social sciences ☐ Ecological, evolutionary & environmental sciences

For a reference copy of the document with all sections, see nature.com/documents/nr-reporting-summary-flat.pdf

Life sciences study design

All studies must disclose on these points even when the disclosure is negative.

Sample size	Sample sizes were predetermined from past experiments, to obtain statistically significant data.
Data exclusions	No mice were excluded from the study.
Replication	All in vitro experiments were performed at least twice, for independent confirmation of the results. Mouse tumour studies were done with the reported biological replicates; and for n>7 they include pooled results from multiple independent experiments. All other experiments were done once for each time point with at least three (and in most cases, more than five) biological repeats. All attempts at replication were successful.
Randomization	Mice were randomized into treatment groups, to provide the same mean tumour size at the start of the treatment.
Blinding	No blinding was done for the study.

Reporting for specific materials, systems and methods

We require information from authors about some types of materials, experimental systems and methods used in many studies. Here, indicate whether each material, system or method listed is relevant to your study. If you are not sure if a list item applies to your research, read the appropriate section before selecting a response.

Materials & experimental systems

n/a	Involved in the study
☐	☒ Antibodies
☐	☒ Eukaryotic cell lines
☒	☐ Palaeontology and archaeology
☐	☒ Animals and other organisms
☒	☐ Human research participants
☒	☐ Clinical data
☒	☐ Dual use research of concern

Methods

n/a	Involved in the study
☒	☐ ChIP-seq
☐	☒ Flow cytometry
☒	☐ MRI-based neuroimaging

Antibodies

Antibodies used	Flow cytometry: antibodies to CD8α (53-6.7), CD103 (2E7), Ly6C (HK1.4), F4/80 (BM8), CD11b (M1/70), CD86 (GL1), MHC2 or I-A/I-E (M5/114.15.2), CD24 (30-F1), CD11c (N418), CCR7 (4B12), CD169 (3D6.112), Ly6G (1A8), CD3 (17A2), NKp46 (29A1.4), Ki67 (16A8), NK1.1 (PK136), Tim3 (RMT3-23), Granzyme B (QA17A02), FoxP3 (MF14), CD44 (1M7), IFN-γ (XMG1.2), CD107a (1D4B), CD62L (MEL-14), CD25 (PC61) and TNFα (MP6-XT22) were obtained from Biolegend. Antibodies to CD45 (30-F11), CD8α (53-6.7) and CD4 (GK1.5) were purchased from BD Biosciences. All antibodies were diluted 1:100. Gp70 tetramer (T-Select H-2Ld MuLV gp70 Tetramer-SPSYVYHQF-PE) was purchased from MBL. Tetramer staining was performed in buffer containing 50 nM dasatinib with 1:50 antibody dilution. Viability was assessed using Zombie Aqua and UV (Biolegend, 1:1000) for tumour and dLN samples or using DAPI for tetramer staining of blood samples. Intracellular staining for FoxP3, Ki67, IFN-γ, TNFα and Granzyme B was performed using the FoxP3 Transcription Factor Buffer Set (eBioscience).

For histology, BV421 anti-mouse CD11b antibody (clone M1/70, Biolegend) and APC anti-mouse CD8α Ly 2 (clone CT-CD8a, Cedarlane) were used with dilution 1:100. For ELISA, anti-mouse IgG-HRP antibody (Biolegend) was used with a 1:5000 dilution and for western blot, a rabbit anti-pSer antibody (Abcam, ab9332, 1:125) and anti-rabbit IR800 antibody (LI-COR, 1:10000) with indication dilution ratios. All other antibodies used for ELISA/ELISPOT purposes were from commerical kits cited in Methods.

For treatments, anti-PD1 (clone 29F.1A12, BioXCell) and TA99 (synthesized in-house) were used at 200 ug per i.p. dose. Depletions of immune cells were done using antibodies against CD8α (clone 2.43, BioXCell 400 ug i.p. twice weekly), NK1.1 (clone PK136, BioXCell, 400 ug i.p. twice weekly), Ly6g (clone 1A8, BioXCell, 400 ug i.p. twice weekly) or CSF1R (clone AFS98, BioXCell, 300 ug i.p. every other day) as previously described. Cytokine neutralization was done using i.p. treatments with 200 ug of antibodies against IFN-γ (clone XMG1.2, BioXCell), IL-1b (clone B122, BioXCell) and IL-18 (clone YIGIF74-1G7, BioXCell) every other day.

Validation

All antibodies other than TA99 were validated by the vendors: Biolegend, BD Biosciences, ThermoFisher, Abcam and BioXCell. TA99 was synthesized in-house and validated by a flow cytometry B16F10 binding assay and in a previous publication (Momin et al., Sci. Transl. Med. 11, eaaw2614 (2019)).

Eukaryotic cell lines

Policy information about cell lines

Cell line source(s)

Cell lines B16F10 (ATCC), HEK-Blue IL-12 (Invivogen), HEK293-F (Gibco), 4T1 (ATCC) and CTLL-2 (ATCC) cells were cultured following vendor instructions. 4T1-GFP-Luc (4T1-Luc) cells were generated by transfection of the 4T1 cell line with pGreenFire lentiviral vector (System Biosciences) and B16F10-Trp2 KO cells were generated as previously described (Moynihan et al). Ag104A, MC38 and B16F10-Zsgreen cells were a gift from H. Schreiber (University of Chicago), J. Schlom (National Cancer Institute) and R. Hynes (MIT) respectively. 4T1 cells were cultured in Roswell Park Memorial Institute (RPMI) 1640 media (ATCC) supplemented with 10% fetal bovine serum (FBS), 100 units/ml penicillin and 100 ug/ml streptomycin while Ag104A, MC38 and B16F10-Zsgreen were all cultures in complete Dulbecco's Modified Eagle's Medium (DMEM) supplemented with 10% fetal serum (FBS), 100 units/ml penicillin and 100 ug/ml streptomycin.

Authentication

Each cell line was maintained separately and stocked in early passages, to minimize contamination and to preserve cell identity.

Mycoplasma contamination

All cell lines that were inoculated in mice were confirmed to be absent of mycoplasma contamination by PCR.

Commonly misidentified lines
(See ICLAC register)

No commonly misidentified cell lines were used.

Animals and other organisms

Policy information about studies involving animals; ARRIVE guidelines recommended for reporting animal research

Laboratory animals

Female C57BL/6 (Taconic, C57BL/6NTac), Balb/C (JAX, 000651), Batf3–/– (JAX, 013755), Nlrp3–/– (JAX, 021302), albino B6 (JAX, 000058), C3H/Hej (JAX, 000659) and IFNγ-reporter GREAT (JAX, 017581) mice at 6–10 weeks age (~20 g) were purchased and maintained in the animal facility at the Massachusetts Institute of Technology.

Wild animals

The study did not involve wild animals.

Field-collected samples

The study did not involve samples collected from the field.

Ethics oversight

All animal studies and procedures were carried out following federal, state and local guidelines under an animal protocol approved by the institutional animal care and use committee at MIT.

Note that full information on the approval of the study protocol must also be provided in the manuscript.

Flow Cytometry

Plots

Confirm that:

☒ The axis labels state the marker and fluorochrome used (e.g. CD4-FITC).

☒ The axis scales are clearly visible. Include numbers along axes only for bottom left plot of group (a 'group' is an analysis of identical markers).

☒ All plots are contour plots with outliers or pseudocolor plots.

☒ A numerical value for number of cells or percentage (with statistics) is provided.

Methodology

Sample preparation

B16F10 tumours and dLNs were harvested 1, 3, 6 or 9 days after i.t. treatment of day-8 tumours. Both were mechanically digested through 70-um nylon cell strainers to prepare single-cell suspensions. Peripheral blood was collected by submandibular bleeding into K2-EDTA tubes (Greiner-Bio), and red blood cells were lysed in ACK Lysis Buffer (Gibco). All samples were then resuspended in ice-cold PBS containing 1% (w/v) BSA and 2 mM EDTA (FACS buffer) with precision count beads (Biolegend, normalized to the weight of tissue per sample) before staining. For intracellular cytokine/granule staining

	of tumour and dLN infiltrating cells, digested tissue samples were resuspended in RPMI supplemented with 10% FBS, 1% penicillin-streptomycin, 1X non-essential amino acids (Invitrogen), 1X sodium pyruvate (Invitrogen), 1X 2-mercaptoethanol (Invitrogen) and 5 ug/mL brefeldin A (Sigma-Aldrich) for 4 hours at 37 °C prior to staining.
Instrument	Cells were analysed using BD FACS LSR Fortessa, or BD FACS Symphony A3 flow cytometers.
Software	BD FACSDiva (BD Biosciences) was used for the collection of FACS data, and FlowJo was used for analysis. The collected data were plotted with statistical analysis by GraphPad Prism.
Cell population abundance	No sorting was used in this study.
Gating strategy	For Fig 5 and Extended Data Figs. 6 and 8, representative gating is provided in Extended Data Fig. 7. IFNγ, Granyzme B positive gating is shown in Fig 5g. For Fig. 6 and Extended Data Fig. 11, representative gating is provided in Extended Data Fig. 10. Zsgreen, CD86-positive gating is presented in Fig. 6b,f, whereas MHC2+ gating is presented in Extended Data Fig. 11d,f. For Fig. 4k, RBCs were gated out using a FSC/SSC plot; subsequently, single cells were gated using a FCA/FCH plot. Live cells were gated using DAPI. Cells were then gated for CD8-positive cells; tetramer-positive gating is depicted in Fig. 4j.

☒ Tick this box to confirm that a figure exemplifying the gating strategy is provided in the Supplementary Information.